Theses and Dissertations   1. Thesis and Dissertation Collection, all items

2019-06

IMPLEMENTATION OF A MICROTURBINE IN A HYDROGEN ENERGY STORAGE AND GENERATION SYSTEM

Kaufmann, Brianna M.

Monterey, CA; Naval Postgraduate School

http://hdl.handle.net/10945/62733

NAVAL POSTGRADUATE SCHOOL

MONTEREY, CALIFORNIA

THESIS

IMPLEMENTATION OF A MICROTURBINE IN A HYDROGEN ENERGY STORAGE AND GENERATION SYSTEM

by

Brianna M. Kaufmann

June 2019

Thesis Advisor: Anthony J. Gannon
Co-Advisor: Andrea D. Holmes

THIS PAGE INTENTIONALLY LEFT BLANK

1. AGENCY USE ONLY *(Leave blank)*	2. REPORT DATE June 2019	3. REPORT TYPE AND DATES COVERED Master's thesis	
4. TITLE AND SUBTITLE IMPLEMENTATION OF A MICROTURBINE IN A HYDROGEN ENERGY STORAGE AND GENERATION SYSTEM		**5. FUNDING NUMBERS** N0001419WX00538	
6. AUTHOR(S) Brianna M. Kaufmann			
7. PERFORMING ORGANIZATION NAME(S) AND ADDRESS(ES) Naval Postgraduate School Monterey, CA 93943-5000		**8. PERFORMING ORGANIZATION REPORT NUMBER**	
9. SPONSORING / MONITORING AGENCY NAME(S) AND ADDRESS(ES) Office of Naval Research, Arlington, VA 22203; ESTEP		**10. SPONSORING / MONITORING AGENCY REPORT NUMBER**	
11. SUPPLEMENTARY NOTES The views expressed in this thesis are those of the author and do not reflect the official policy or position of the Department of Defense or the U.S. Government.			
12a. DISTRIBUTION / AVAILABILITY STATEMENT Approved for public release. Distribution is unlimited.		**12b. DISTRIBUTION CODE** A	

13. ABSTRACT (maximum 200 words)

The energy needs of the Navy and the Department of Defense demand renewability, reliability, and resilience. Diverse means of energy production, including hydrogen gas combustion, support these requirements. The overarching goal of this research is to develop a system that produces and stores hydrogen and then combusts the hydrogen in a commercial microturbine to produce electricity. This thesis focuses on fueling a Capstone C30 MicroTurbine with hydrogen. Future research will produce a complete system that uses renewable resources, reliably produces electricity to meet demand, and demonstrates fuel resiliency.

The implementation of the C30 enables the use of a renewable resource in a reliable and resilient system. A system component with the capability to produce energy from hydrogen (in addition to methane and propane) indicates resilience in fuel choices. If the primary fuel is unavailable, secondary fuels fulfill the demand for energy. Resilient technologies must use several fuels with varying properties. Computational fluid dynamic models establish expected operating differences between different types of fuel. Data collected from the C30 establish operating differences between light hydrocarbon fuels (natural gas, propane) and hydrogen gas. Benefits and challenges of using hydrogen gas-fueled microturbines and recommended improvements are discussed.

14. SUBJECT TERMS energy, resilience, reliability, renewable, hydrogen, gas turbine, microturbine, energy resilience, renewable energy			**15. NUMBER OF PAGES** 103
			16. PRICE CODE
17. SECURITY CLASSIFICATION OF REPORT Unclassified	**18. SECURITY CLASSIFICATION OF THIS PAGE** Unclassified	**19. SECURITY CLASSIFICATION OF ABSTRACT** Unclassified	**20. LIMITATION OF ABSTRACT** UU

THIS PAGE INTENTIONALLY LEFT BLANK

IMPLEMENTATION OF A MICROTURBINE IN A HYDROGEN ENERGY STORAGE AND GENERATION SYSTEM

Brianna M. Kaufmann
Ensign, United States Navy
BS, U.S. Naval Academy, 2018

Submitted in partial fulfillment of the
requirements for the degree of

MASTER OF SCIENCE IN MECHANICAL ENGINEERING

from the

**NAVAL POSTGRADUATE SCHOOL
June 2019**

Approved by: Anthony J. Gannon
                Advisor

                Andrea D. Holmes
                Co-Advisor

                Garth V. Hobson
                Chair, Department of Mechanical and Aerospace Engineering

iii

THIS PAGE INTENTIONALLY LEFT BLANK

ABSTRACT

The energy needs of the Navy and the Department of Defense demand renewability, reliability, and resilience. Diverse means of energy production, including hydrogen gas combustion, support these requirements. The overarching goal of this research is to develop a system that produces and stores hydrogen and then combusts the hydrogen in a commercial microturbine to produce electricity. This thesis focuses on fueling a Capstone C30 MicroTurbine with hydrogen. Future research will produce a complete system that uses renewable resources, reliably produces electricity to meet demand, and demonstrates fuel resiliency.

The implementation of the C30 enables the use of a renewable resource in a reliable and resilient system. A system component with the capability to produce energy from hydrogen (in addition to methane and propane) indicates resilience in fuel choices. If the primary fuel is unavailable, secondary fuels fulfill the demand for energy. Resilient technologies must use several fuels with varying properties. Computational fluid dynamic models establish expected operating differences between different types of fuel. Data collected from the C30 establish operating differences between light hydrocarbon fuels (natural gas, propane) and hydrogen gas. Benefits and challenges of using hydrogen gas-fueled microturbines and recommended improvements are discussed.

THIS PAGE INTENTIONALLY LEFT BLANK

TABLE OF CONTENTS

LIST OF FIGURES

LIST OF TABLES

THIS PAGE INTENTIONALLY LEFT BLANK

LIST OF ACRONYMS AND ABBREVIATIONS

C30	Capstone Turbine Corporation C30 MicroTurbine
CFD	computational fluid dynamics
CH_4	methane gas
C_3H_8	propane gas
COTS	commercial off-the-shelf
CRMS	Capstone Remote Monitoring System
DoD	Department of Defense
DoN	Department of the Navy
H_2	hydrogen gas
K	Kelvin
kg/s	kilogram per second
kPa	kilopascal
kW	kilowatts
m/s	meters per second
NPS	Naval Postgraduate School
RPM	revolutions per minute
s	seconds
TET	turbine exit temperature
TPL	Turbopropulsion Laboratory

THIS PAGE INTENTIONALLY LEFT BLANK

ACKNOWLEDGMENTS

I would like to thank my friends and family for their support during the course of my studies at NPS. A special acknowledgement to my younger brother, MIDN Turner Kaufmann, who inspires me to be a better naval officer every day.

I would like to thank my teachers and mentors at the United States Naval Academy who helped me pursue the Bowman Scholar Program and further education, especially CDR Stuart Blair, PhD, USN.

I would like to thank my advisors, Dr. Anthony Gannon and Ms. Holmes, for their technical expertise, leadership, and patience. Mr. John Gibson provided key technical support and, last but not least, I would like to thank Dr. Garth Hobson for the vision for this research project.

THIS PAGE INTENTIONALLY LEFT BLANK

I. INTRODUCTION

The energy needs of the Department of the Navy (DoN) and the Department of Defense (DoD) demand renewability, reliability, and resilience. Diverse means of energy production support these requirement, including hydrogen gas (H_2) combustion. This thesis is one of several researching and developing a H_2 energy storage and generation system.

A. MOTIVATION

H_2 combusts in air to produce heat like gaseous hydrocarbons such as methane (CH_4, the primary component of natural gas) or propane (C_3H_8). However, H_2 produces more energy per unit mass and emits no carbon compounds. Figure 1 visually compares lower heating values (LHV) of mass energy densities. Existing renewable and reliable production methods enable the development of energy resilience with respect to hydrogen-based systems [1].
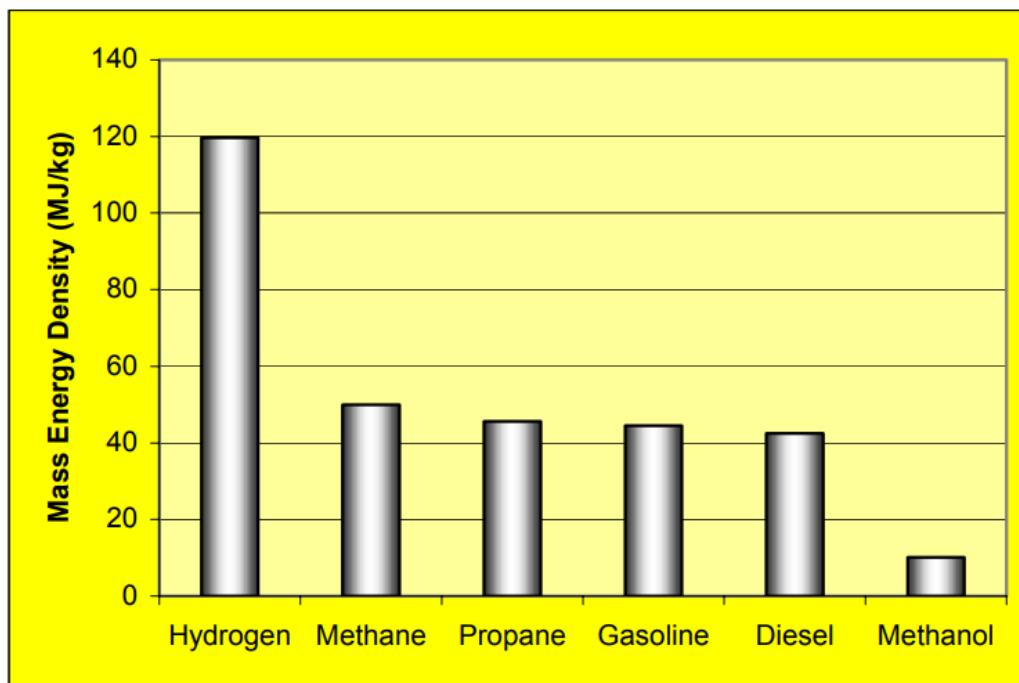
Figure 1.   Mass energy densities of various fuels (LHV) Source: [2].

Recent policy takes a two-pronged approach to energy: first, reduce energy use and second, implement renewable energy technologies where energy use is required. The Energy Policy Act of 2005 focuses on reduced energy use [3]. Among the renewable energy technologies discussed in the act, Title VIII specifically discusses the purposes of hydrogen and hydrogen fuel cells: "to sharply decrease the dependency of the United States on imported oil, eliminate most emissions from the transportation sector, and greatly enhance our energy security and…to create, strengthen, and protect a sustainable national energy economy" [3]. H_2 has been recognized as an energy source for many years, but the enabling technology required for robust and interconnected systems requires more research.

This thesis builds on the work of several other theses. Previous work examined H_2 generation via solar power, automated the production and storage process, and fueled a small turbojet engine with H_2 [4]–[7]. This work focuses on testing a commercial off-the-shelf (COTS) microturbine with H_2 for implementation in a small H_2 generation, storage, and energy generation system. The implementation of a COTS microturbine in a H_2 system demonstrates the use of a renewable resource in a reliable and resilient system. A component with the capability to produce energy from H_2 (in addition to CH_4 and C_3H_8) indicates resilience in fuel choices. If the primary fuel is unavailable, secondary fuels fulfill the demand for energy. This work is sponsored by the Office of Naval Research Energy Systems Technology Evaluation Program under the technical monitoring of Marissa Brand. This research intends to contribute to the efforts of the DoD and DoN to use more renewable energy to increase energy resilience.

B. OBJECTIVES

The primary objective of this research is to fuel a COTS microturbine with H_2, demonstrating its role in a larger renewable energy system and ultimately a hydrogen economy. The specific COTS microturbine used is the Capstone Turbine Corporation's C30 MicroTurbine (C30). The secondary objective is to make design recommendations for improved operation with H_2. Enabling objectives include:

1. Installing a low pressure natural gas supply line;

2. Constructing self-contained fuel supply systems for both C_3H_8 and H_2;

3. Implementing remote monitoring software to collect real-time data from the C30;

4. Fueling the COTS microturbine with natural gas and collecting data;

5. Fueling the COTS microturbine with C_3H_8 and collecting data;

6. Developing a computational fluid dynamics (CFD) model of H_2, natural gas, and C_3H_8 combustion processes.

C. BACKGROUND AND LITERATURE REVIEW

The development of a hydrogen economy is predicted to most heavily impact the transportation, grid services, and some "niche markets" including "remote and backup power" systems [8]. Because this thesis focuses on using small gas turbine technology to produce electricity, emphasis is placed on the significance of grid electricity on the microgrid scale. Melaina [8] specifically identifies turbines as an enabling technology to overcome the challenges of a H_2 grid: "The conversion of hydrogen back to grid electricity … is challenging economically for grid-connected systems because of significant energy losses. Where reconversion to grid electricity is viable, it may be achieved by using either stationary fuel cells or thermal conversion units, *such as turbines*" (emphasis added). More research is required to develop economically viable large-scale H_2 grids; smaller or more isolated grids are suited to H_2 fuel.

Current means of H_2 production, storage, and transportation are the limiting factors of wide distribution to economically viable large-scale grids. Smaller grids address production and storage on-site and reduce or eliminate transportation demands. Today, the majority of industrial H_2 production "is by steam reforming of the natural gas, and gives rise to a lot of carbon dioxide" [9]. Large volumes of H_2 are produced via electrolysis of water on U.S. Navy submarines, but because oxygen is the only desired result, H_2 is dumped overboard. Instead of fossil fuels and discarded H_2, production means are focused on electrolysis using electricity from renewable sources [1]. Levene describes the vast resources of solar and wind energy as mathematically feasible for H_2 production: "certainly enough renewable energy resources exist to provide the electricity needs for renewable hydrogen generation, but the most economic configuration has yet to be identified" [1]. The current system at the Naval Postgraduate School (NPS) Turbopropulsion Laboratory (TPL) uses solar power, photovoltaic cells, and dehumidifiers to produce H_2 from atmospheric water using only renewable energy [4]–[6]. The electrolysis process is well-understood but not yet implemented on a large- and/or economically feasible scale. However, at high temperatures (between 700ºC and 900ºC) electrolysis becomes more thermodynamically favorable and at even higher temperatures (above 900 ºC) H_2 may be thermochemically produced [9]. Coupling waste heat-intensive renewable and/or carbon-neutral energy production (e.g., nuclear power) with H_2 production may make H_2 more economically feasible [9].

Storage challenges compound the challenges of production. Although H_2 has a high mass energy density, its volumetric energy density pales in comparison to heavier hydrocarbon fuels. Figure 2 visually compares the LHV of volumetric energy densities of various fuels. Even liquid H_2 struggles to attain a third of the energy per unit volume that liquid gasoline or liquid diesel can provide [2].
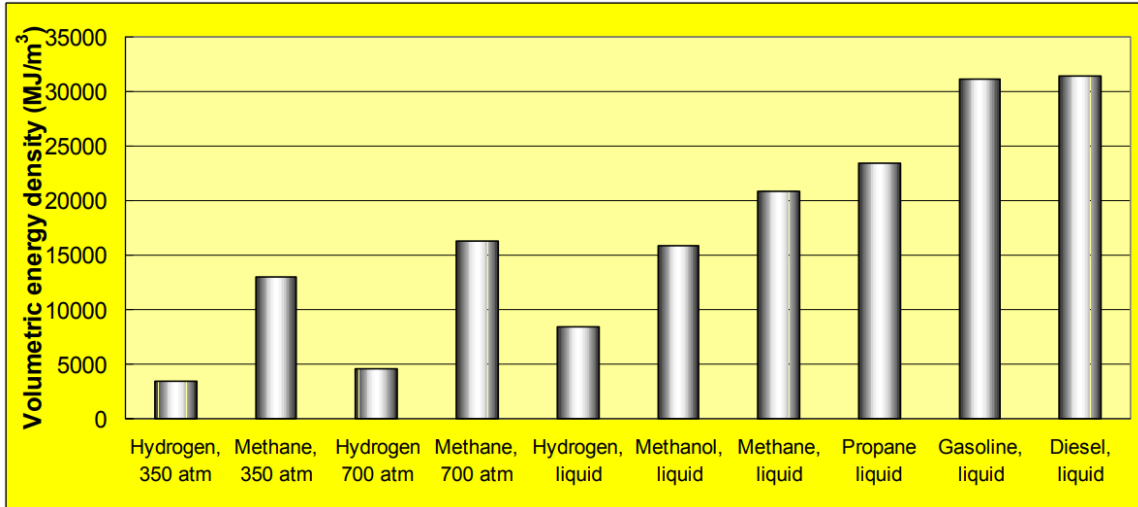
Figure 2.   Volumetric energy densities of various fuels (LHV)
Source: [2].

H_2 may be stored in gaseous form, liquid form, or within solid media [2]. Metallic cylinders (typically steel or aluminum) can store H_2 at high pressures and atmospheric temperatures. These cylinders are compact and portable but contain only small amounts of H_2; additionally, over long-term use "hydrogen may degrade the mechanical behavior of metallic materials used in the hydrogen infrastructure (e.g., storage tanks)" [2]. Liquid storage requires moderate pressures and low temperatures. The Linde cycle and the Claude cycle are two common methods of liquefaction but require significant amounts of energy [2]. Solid media include metal hydrides, non-carbon porous materials, and new materials such as boron nitride nanotubes [2]. Although these media have potential for improved volumetric storage capacity at low pressures, the technologies are not yet mature and face weight-to-power ratio drawbacks [2]. The current system at the TPL and this research store and use H_2 in gaseous form [4]. For the same reasons of material degradation and volumetric energy density, continuously transporting large masses of H_2 over long distances becomes challenging.

Despite these infrastructure challenges, H_2 combustion has undisputable benefits of being emissions-free and completely renewable. The DoD and DoN have invested in hydrogen-based technologies and support research to develop a hydrogen economy. This research contributes to one small aspect of a larger effort.

5

D.   APPROACH

This thesis approached the challenges of increasing energy resilience and using H_2 in a microgrid by testing the feasibility of fueling a COTS microturbine with H_2. Simulation used computational fluid dynamics (CFD) tools to predict the different volumetric flow rates required for and temperatures produced during combustion of C_3H_8, natural gas, and H_2. Experimental testing began with baseline performance of the C30 using the specified fuels of natural gas and C_3H_8 and proceeded to testing with H_2.

II. SIMULATION

Because H_2 is less dense at the same temperature and pressure and has different properties from current hydrocarbon fuels (CH_4, C_3H_8, kerosene, etc.), simulation is necessary to predict the effects of using a different fuel than the power generation system specifies. For example, fuel nozzle designs take into account the mass and volumetric flow rates and the laminar flame speed of the intended fuel. Two programs modeled aspects of the C30's expected performance using H_2: the ANSYS CFX suite and GasTurb 11.

A. ANSYS CFX CFD COMBUSTION SIMULATION

The ANSYS CFX suite of combustion simulation tools developed a CFD simulation of H_2 burning in air in a combustion chamber. The information gained from the simulation predicted some of the effects of using H_2 in the fuel nozzles and combustion chamber and the associated possible technical design changes. The C30 has a fuel nozzle and combustion chamber indicated for use with C_3H_8 or natural gas. Future power generation systems will require redesigned or improved fuel nozzles indicated for use with one or more types of fuels, including H_2.

Using the principles contained within "Chapter 20: Radiation and Combustion in a Can Combustor" of ANSYS CFX Tutorials, 16th ed. and guidance from ANSYS CFX-Solver Theory Guide, 15th ed., a model of a generic fuel nozzle was developed and evaluated for C_3H_8-air combustion [10], [11]. Subsequently, the performance of the same nozzle with CH_4-air combustion and H_2-air combustion was evaluated. CH_4 is the simplified composition of natural gas for the purposes of this simulation. In Chapter IV, Section B natural gas test runs are labeled "CH_4" for brevity and to identify CH_4 as the primary component of natural gas.

Data on fuel inlet velocity, maximum temperature achieved, and mass air-fuel ratios were collected and compared for each fuel type. Design improvements to the fuel nozzle for use with H_2 were recommended.

7

1. Procedure

The following procedure is paraphrased from chapter 20 of the ANSYS CFX Tutorials [10].

1. Create a standalone CFX system in the ANSYS Workbench environment.

2. Download the *CombustorMesh.gtm* mesh file from the ANSYS Customer Portal and import the mesh into standalone CFX system. The provided mesh was determined to have sufficient resolution and was unchanged.

3. Create a reacting variable composition mixture by selecting the appropriate H_2 -, CH_4-, or C_3H_8-air reacting mixture. The mixtures are simplified: the "NO PDF reaction specifies complete combustion of the fuel into its products in a single-step reaction" [10]. Additionally, "setting the radiation properties explicitly will significantly shorten the solution time" [10]. These selections reduce the computational and time demands of the simulation without significantly affecting the result [11].

4. Develop the simulation domain and create boundaries of the following types: inlet, outlet, and wall. This process establishes the fuel and air flow paths. The independent variable controlled in this simulation is the fuel inlet velocity. Use the default k-ε turbulence model and the default turbulence intensity option, Medium (Intensity = 5%).

5. Set the solver control settings. The tutorial recommends a maximum of 100 iterations and a physical timescale of 0.025 seconds (s). However, the physical time step was changed to 0.015 s, the maximum iterations to 500, and the RMS to 1e-5 to ensure convergence of the solution.

6. Obtain the solution and collect the specified data. The data collected included the fuel inlet velocity and a map of the temperatures achieved inside the combustion chamber. Additionally, ANSYS's function calculator collected mass flow rates at the fuel inlet and both the primary and secondary air inlets. The actual mass air-fuel ratio and the

8

stoichiometric air-fuel ratio were compared for each air-fuel mixture and inlet velocity.

7.   Repeat steps 3 through 6 until all data has been collected for the desired fuel inlet velocities and fuel-air mixtures.

2.   Propane-Air Combustion (Eddy Dissipation Model)

C_3H_8-air combustion occurred with a fuel inlet velocity of 40 meters per second (m/s) [10]. The maximum temperature achieved inside the combustion chamber is 2392.49 Kelvin (K). The mass air-fuel ratio at the inlets is 12.91, less than the amount of air required for a stoichiometric mass air-fuel ratio of 15.67 [12]. This combustion chamber runs rich. The temperature map, shown in Figure 3, reveals turbulent air-fuel mixing and a developed flame that is centered in the combustion chamber but impinges on the combustion chamber walls near the outlet. Temperatures near the combustion chamber side walls are half those found in the flame.
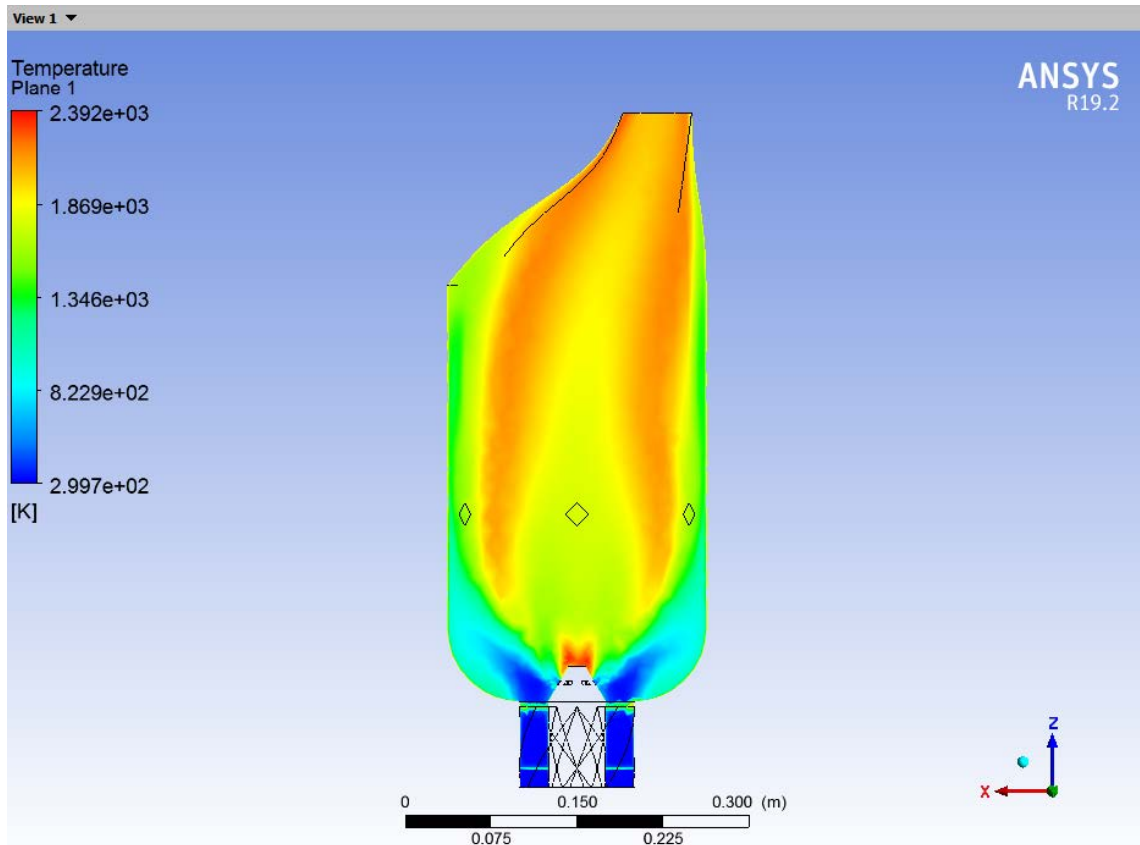
Figure 3.   Temperature inside the combustion chamber (C_3H_8-air reaction, 40 m/s)

In Figure 3 and subsequent temperature maps, ANSYS CFX varies the temperature scales (shown on the left-hand side of each figure) from the maximum to the minimum temperatures achieved in the simulation. The scale changes with each fuel scenario.

Figure 4 shows the fuel mass fraction compared to all combustion products and reactants inside the combustion chamber. Some C_3H_8 is observed leaving the combustion chamber due to the rich mass air-fuel ratio and incomplete combustion. C_3H_8 still undergoing combustion at the combustion chamber outlet may cause a flame to impinge upon the walls of the combustion chamber.

Figure 4.   Fuel mass fraction inside the combustion chamber (C_3H_8-air reaction, 40 m/s)

3.   Methane-Air Combustion (Eddy Dissipation Model)

CH4-air combustion occurred with a fuel inlet velocity of 40 m/s [10]. The maximum temperature achieved inside the combustion chamber is 2225.44 K. The mass air-fuel ratio at the inlet is 35.46, which is approximately twice the amount of air required for a stoichiometric mass air-fuel ratio of 17.19 [12]. This combustion chamber runs lean, typical of most gas turbines. (ANSYS's tutorial specifies the use of CH4; the resulting flame pattern factor and mass air-fuel ratio are ideal for the design of the can combustor [10].) These data support the conclusion that for fuels of a higher volumetric energy density, the volume flow rate must be reduced (e.g., C_3H_8), and that inversely, fuels (e.g., CH4 and H2) with a lower volumetric energy density require an increased volume flow rate [2]. For an inlet orifice of constant area, the same fuel inlet velocity produces the same volumetric flow rate for a fluid. With the same fuel inlet velocity, C_3H_8 and CH4

11

have the same volumetric flow rate. However, the higher volumetric energy density of C_3H_8 produces rich combustion while the lower volumetric energy density of CH_4 produces lean combustion.

The temperature map, shown in Figure 5, reveals turbulent air-fuel mixing and a developed flame that is centered in the combustion chamber and connects near the outlet. Temperatures near the combustion chamber side walls are less than half those found in the flame. This flame-to-wall temperature ratio is slightly higher than the same temperature ratio for C_3H_8. A high temperature ratio, or steeper temperature gradient, between the flame and the walls reduces the thermal load on the materials that comprise the combustion chamber.
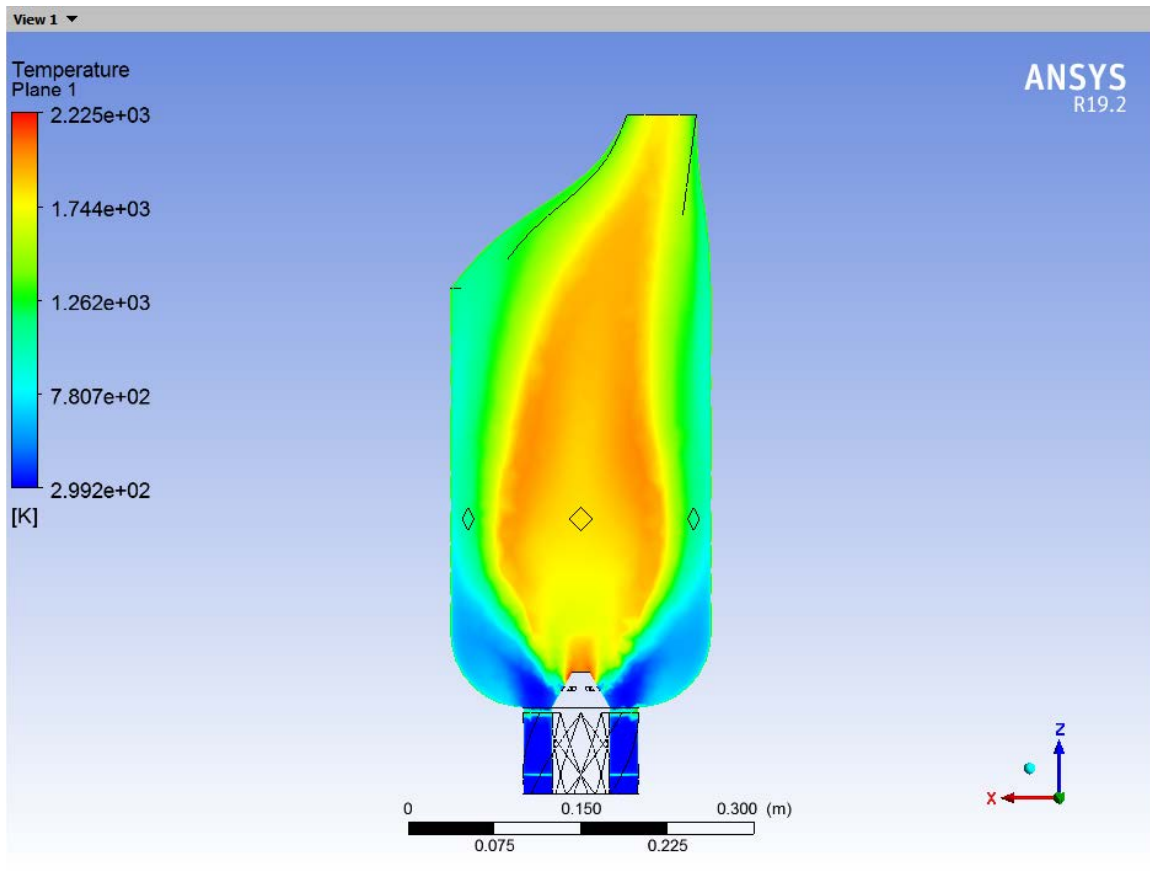
Figure 5.   Temperature inside the combustion chamber (CH_4-air reaction, 40 m/s)

Figure 6 shows the fuel mass fraction compared to all combustion products and reactants inside the combustion chamber. CH_4 is observed to undergo complete combustion. No flame will impinge upon the walls of the combustion chamber.
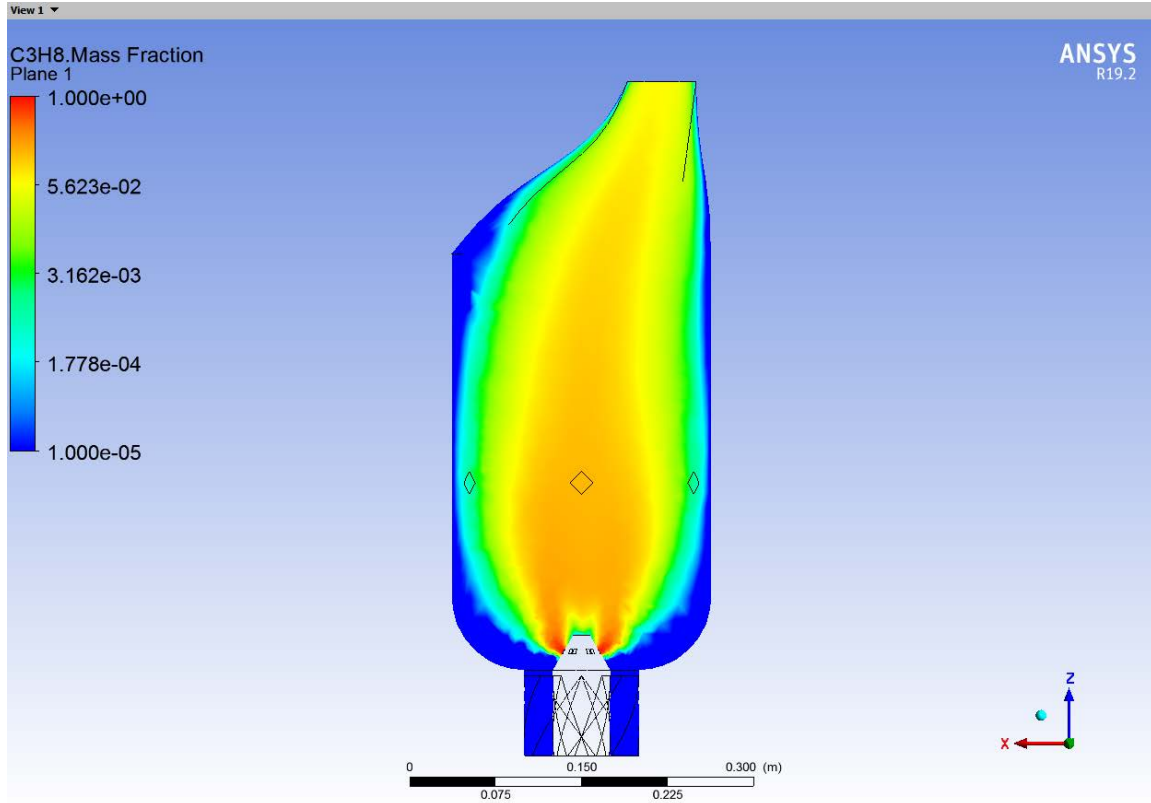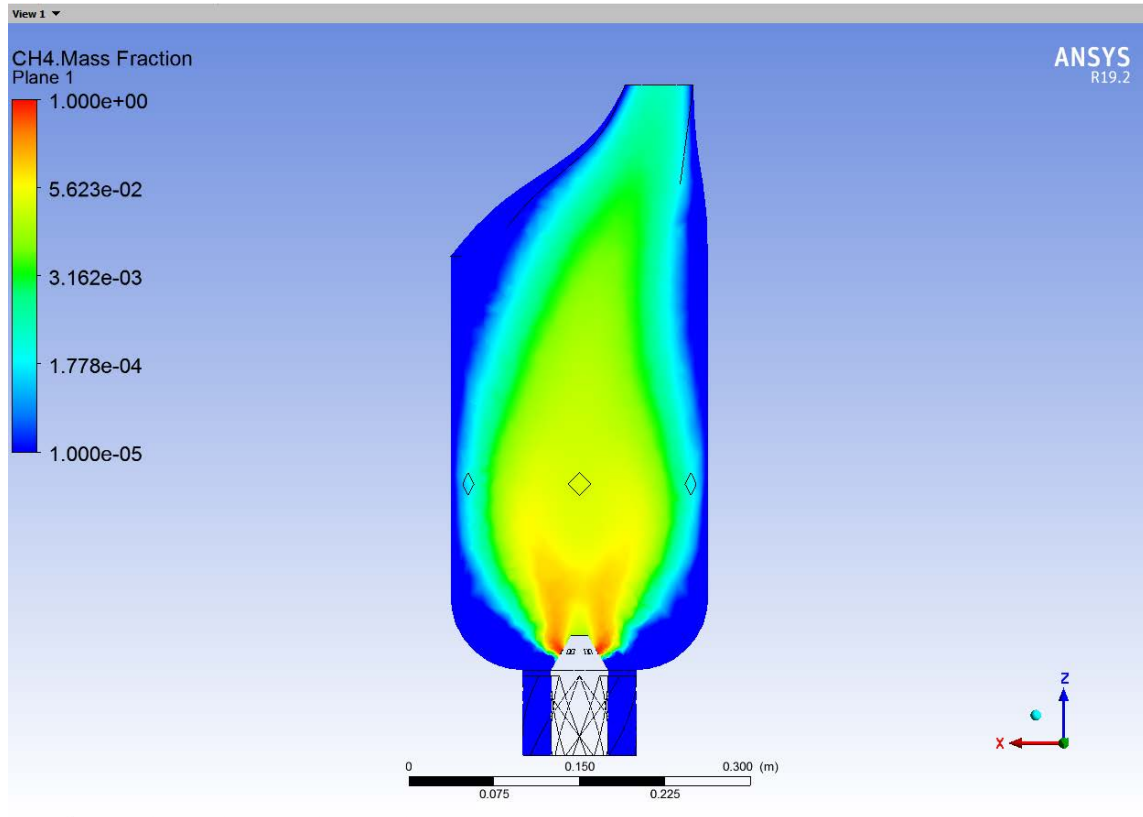

Figure 6.   Fuel mass fraction inside the combustion chamber (CH_4-air reaction, 40 m/s)

4.   Hydrogen-Air Combustion (Eddy Dissipation Model)

H_2-air combustion occurred with a fuel inlet velocity from 10 m/s to 60 m/s in increments of 5 m/s, with an additional data point at 165 m/s. The fuel inlet velocity was varied to determine the volumetric flow rate at which the flame pattern factor and mass air-fuel ratio most resembled operation with CH_4 at a fuel inlet velocity of 40 m/s [10]. Table 1 contains fuel inlet velocities, maximum temperatures, and mass flow ratios for H_2-air combustion. The equivalence ratio compares the simulated mass air-fuel ratio to the stoichiometric mass air-fuel ratio of 34.3 for H_2 [12].

13

Table 1. H_2 -air combustion chamber data

Fuel Inlet Velocity [m/s]	Maximum Temperature [K]	Air-Fuel Mass Flow Ratio [-]	Equivalence Ratio [-]
10	1998.89	1128	32.88
15	1998.97	755.9	22.04
20	2046.59	566.9	16.53
25	1998.45	451.2	13.15
30	2062.56	376.0	10.96
35	2095.34	322.3	9.396
40	2151.32	282.0	8.222
45	2135.68	250.7	7.308
50	2174.83	225.6	6.578
55	2211.87	205.1	5.980
60	2247.90	189.0	5.510
165	2491.92	68.43	1.995

Figure 7 shows the temperature map for a H_2 fuel inlet velocity of 40 m/s (the same fuel inlet velocity tested for CH_4 and C_3H_8). The maximum temperature inside the combustion chamber is 2151.32 K. The mass air-fuel ratio at the inlets is 282.0, which is an order of magnitude higher than the stoichiometric mass air-fuel ratio of 34.3 [12]. This combustion chamber runs lean at all fuel inlet velocities tested. The high laminar flame speed of H_2, coupled with the low volumetric energy density, produces a poorly developed flame [12].
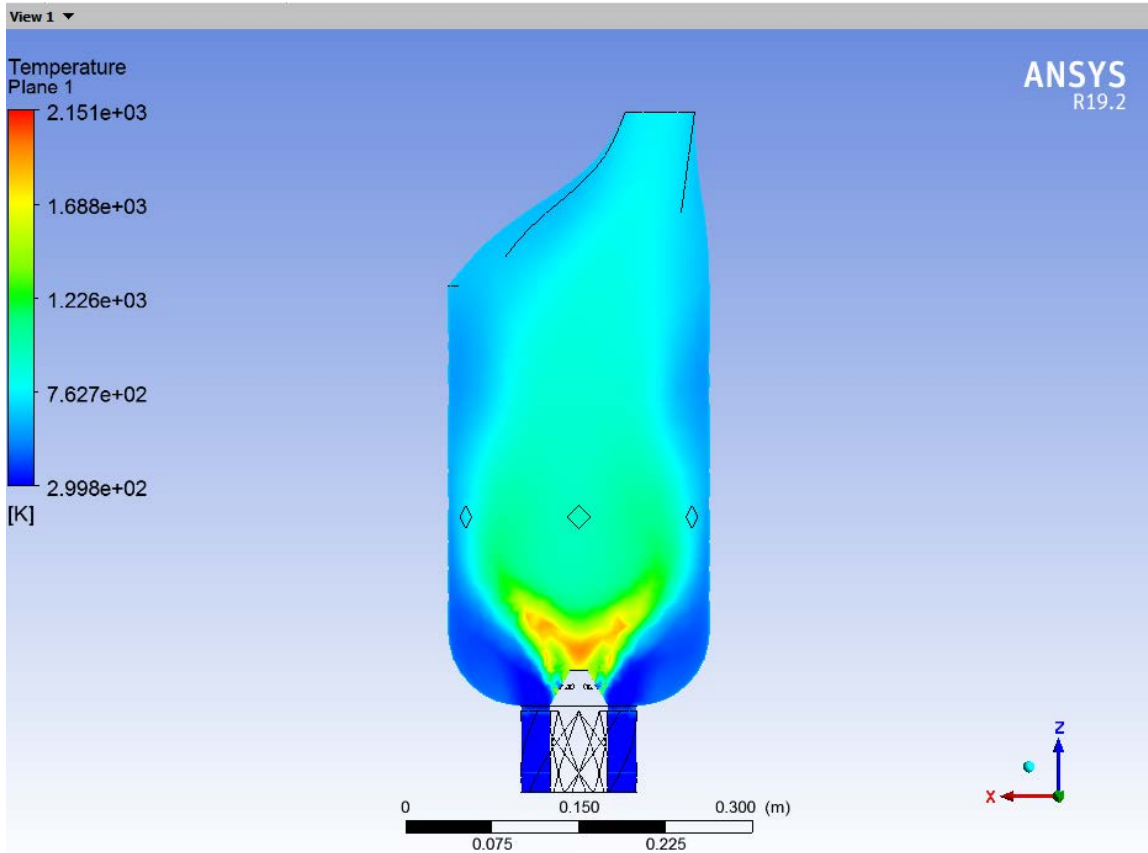
Figure 7.   Temperature inside the combustion chamber (H_2-air
reaction, inlet velocity 40 m/s)

The last row in Table 1 fuels the combustion chamber at a mass air-fuel ratio twice that of the mass air-fuel stoichiometric ratio. This operating point was chosen because the CH_4-fueled chamber uses this mass air-fuel ratio at its design performance. An inversely proportional relationship exists between fuel inlet velocity and the mass air-fuel ratio through a constant cross-sectional area. Extrapolating the results from 10 m/s to 60 m/s, the resulting velocity is 165 m/s. Appendix A contains the pertinent calculations. Additionally, all results from all simulations are tabulated in Appendix B and temperature maps for all fuel inlet velocities simulated are contained in Appendix C. At this velocity, the maximum temperature achieved in the H_2-air combustion chamber is 2491.92 K, 266.48 K higher than the maximum temperature achieved in the CH_4-air combustion chamber at 2225.44 K and 99.43 K higher than the maximum temperature achieved in the

15

C_3H_8-air combustion chamber at 2392.49 K. This combustion chamber runs lean at all fuel inlet velocities tested.

Figure 8 shows the temperature map for a H_2 fuel inlet velocity of 165 m/s (the calculated fuel inlet speed required to maintain a mass air-fuel ratio twice that of the stoichiometric air-fuel ratio). The maximum temperature inside the combustion chamber is 2491.92 K. The mass air-fuel ratio at the inlets is 68.43, which is twice that of the stoichiometric mass air-fuel ratio of 34.3 [12]. This combustion chamber runs lean. The flame reveals turbulent air-fuel mixing and a developed flame that is centered in the combustion chamber and connects near the outlet in a pattern factor similar to that found in the CH_4-fueled combustion chamber. However, temperatures near the combustion chamber side walls are higher than those found in the CH_4-fueled combustion chamber.
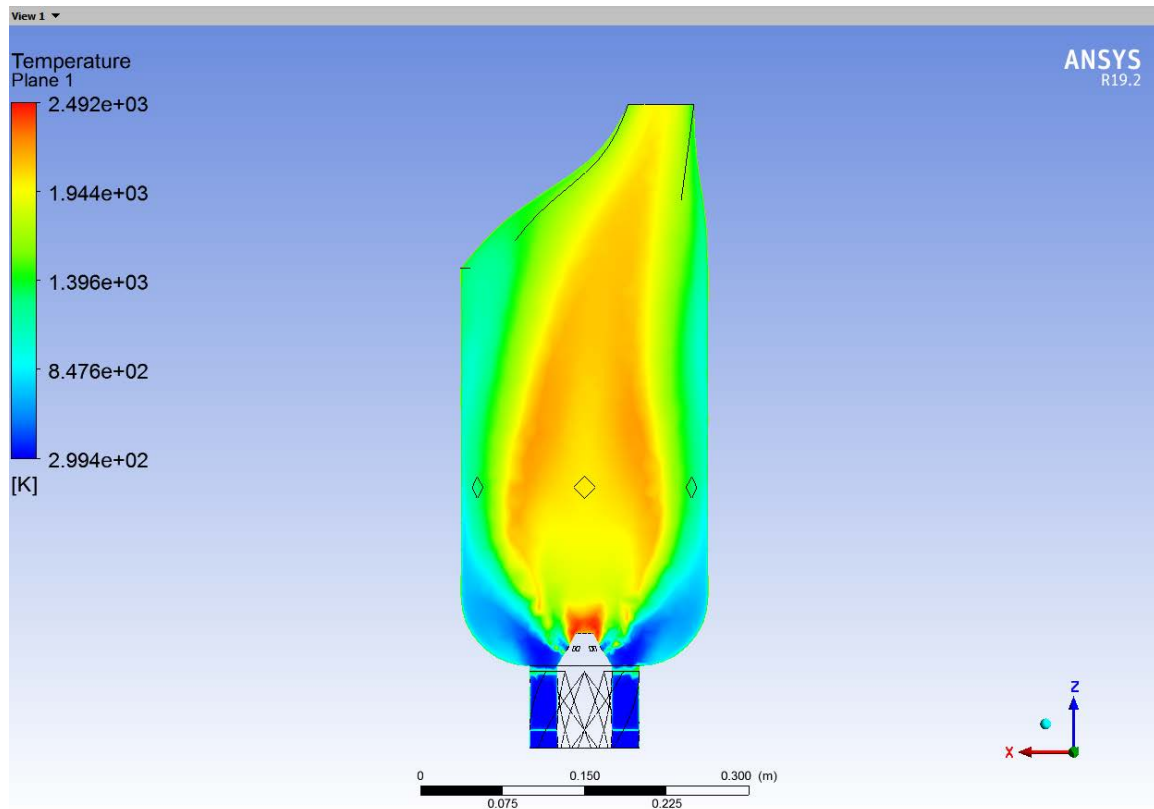
Figure 8.   Temperature inside the combustion chamber (H_2-air reaction, inlet velocity 165 m/s)

There are two challenges associated with the fuel inlet velocity of 165 m/s and resulting temperature. First, as the material composition of this generic combustion chamber is unknown, it is uncertain whether the increased temperature will cause immediate and/or long-term damage to the combustion chamber. A key challenge in using H_2 in the place of light hydrocarbon fuels is the increased flame temperature. The adiabatic flame temperatures of C_3H_8, CH_4, and H_2 in air are 1980 K, 1963 K, and 2254 K, respectively [12]. Second, the fuel nozzle design of this combustion chamber may not be able to supply the H_2 at the required volumetric flow rate.

Figure 9 shows the fuel mass fraction compared to all combustion products and reactants inside the combustion chamber. This data was taken with a fuel inlet velocity at 165 m/s. H_2 is observed to undergo complete combustion, with the fuel mass fraction reaching zero by one-quarter the length of the combustion chamber. No flame will impinge upon the walls of the combustion chamber.
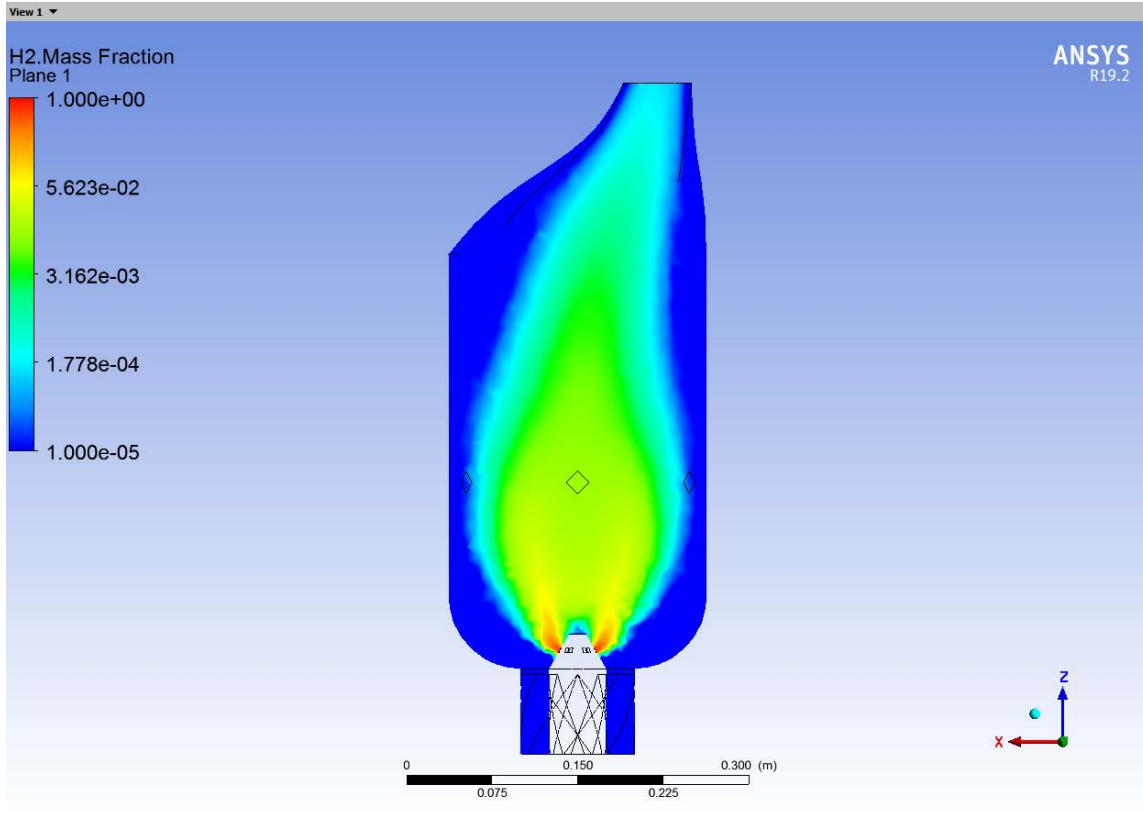
Figure 9.   Fuel mass fraction inside the combustion chamber (H_2-air reaction, 165 m/s)

Figure 10 compares inlet velocity to the resulting maximum temperature in the H_2-air combustion chamber. The maximum temperatures achieved using CH_4 and C_3H_8 are included.
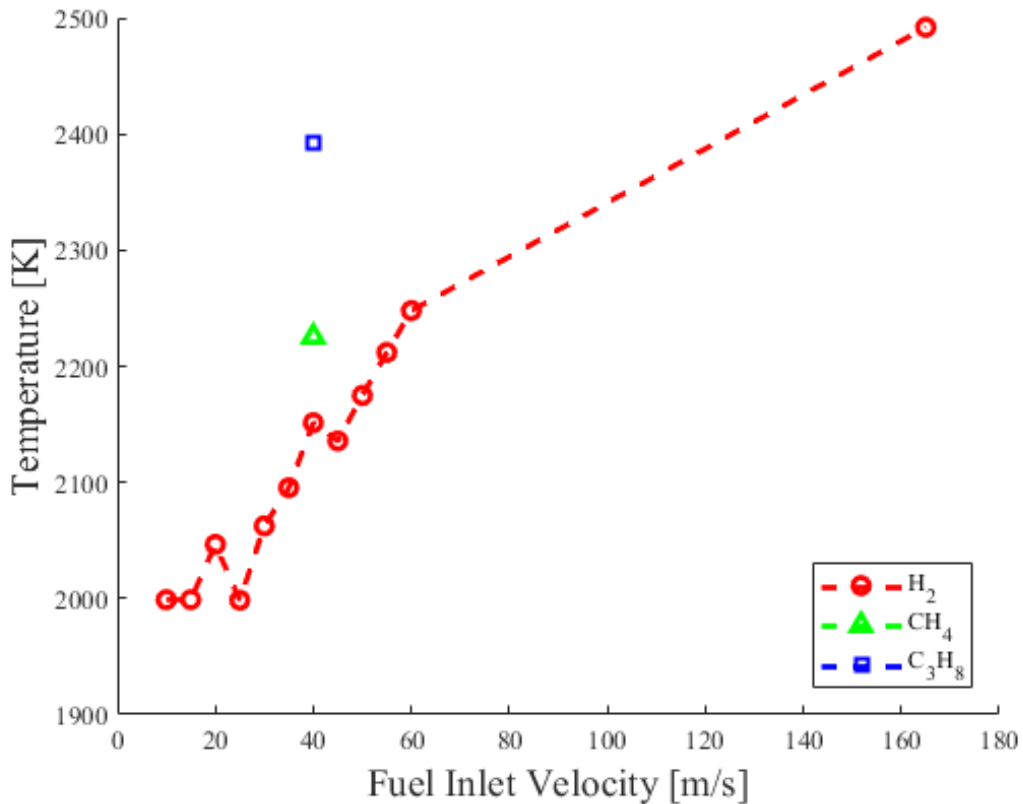
Figure 10.   The maximum temperature achieved correlates with the
fuel inlet velocity

The maximum temperature increases with fuel inlet velocity. For lean combustion, more fuel in the same amount of air will produce more heat. (For the same inlet velocity, CH_4 and C_3H_8 produce more heat because the greater fuel density allows proportionally more fuel.) Due to the unstable nature of the H_2 flame, the maximum temperature achieved is also unstable at low fuel inlet velocities and is not directly proportional to the fuel inlet velocity, as shown.

Figure 11 compares inlet velocity to the mass air-fuel ratio. For a constant inlet velocity, H_2 produces a higher mass air-fuel ratio than CH_4 or C_3H_8 because of its lower density at the same temperature and pressure.
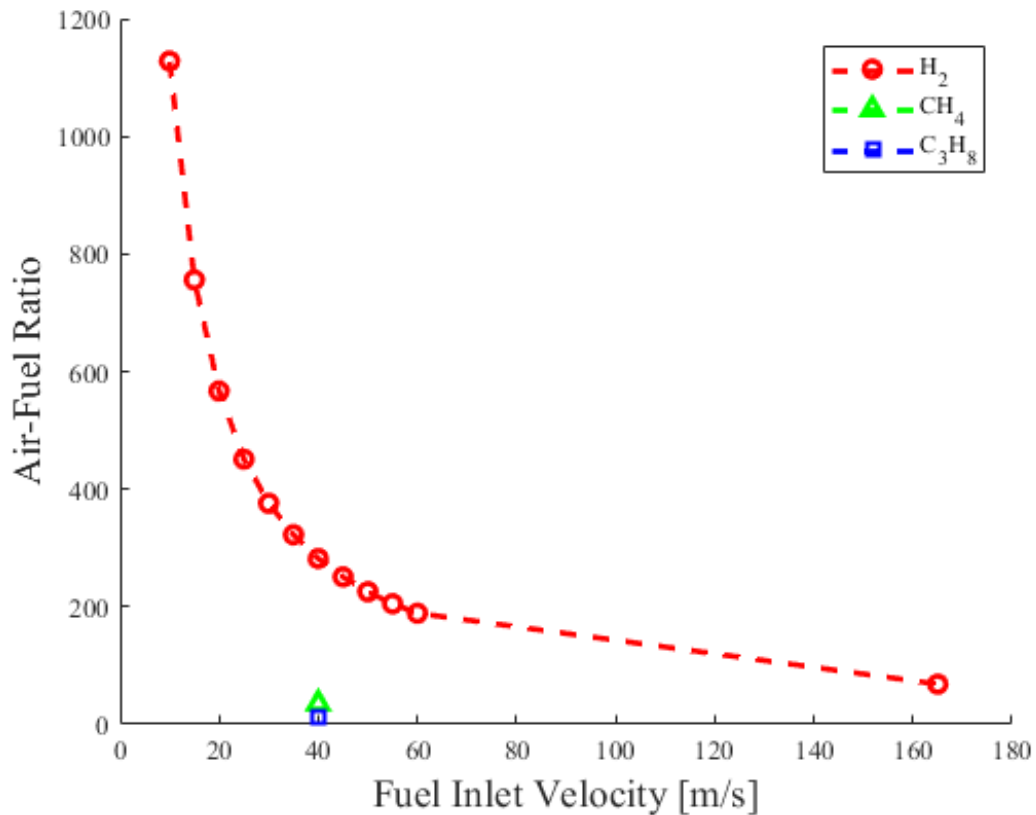
Figure 11.   The mass air-fuel ratio is inversely proportional to the fuel inlet velocity

Future simulation work should redesign the nozzle and ensure that all materials in the combustion chamber are suitable for the increased temperature. This information will contribute to an improved microturbine design for operation with H_2.

B.   GASTURB SIMULATION

GasTurb 11 is a program that allows analysis of gas turbine performance, both on- and off-design, for several types of gas turbines with widely varying parameters. It was

used to model the expected performance and fuel mass flow rate at the full power output, 30 kilowatts (kW), of the C30 using H_2 and natural gas. Although the C30 was only tested at idle speeds, this model predicted the change in fuel demands as a function of different types of fuel. Appendix D contains the full input decks used and several output decks.

1. Data Input

The C30 specifications identified in the thermodynamic model validation by Gimelli and Sannino were used to develop data inputs for GasTurb [13]. The inputs and GasTurb program environment are shown in Figure 12. For these same inputs, the drop-down menu was used to select natural gas or H_2 fuel. Then a single on-design cycle was run and data was collected.

Figure 12. GasTurb 11 input parameters using H_2

2.   Data Output and Results

For natural gas, the calculated fuel mass flow rate was 0.00230 kilograms per second (kg/s). H_2 produced a fuel mass flow rate of 0.00095548 kg/s. Both data points were simulated at full power (30 kW) although experimental testing was only completed at idle speeds and no power output. These calculations confirm the high mass energy density of H_2 compared to natural gas and also present an upper bound on the expected fuel consumption during test runs of the C30. Figure 13 shows a temperature-entropy plot of the C30 simulated with H_2.
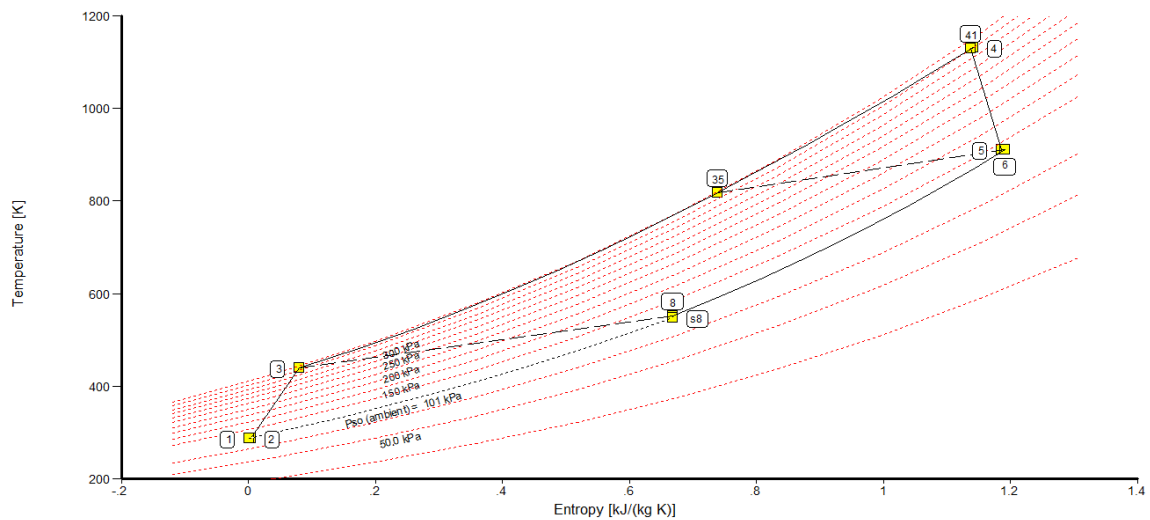
Figure 13.   GasTurb 11 output temperature-entropy plot using H_2

III.   SYSTEM DESIGN

Previous research focused primarily on the production, compression, and storage of H_2 [4]–[6]. Beginning with Penley's research on the operation of a small gas turbine, each power generation system required the construction of a fuel supply system [7]. This research used C30 engines and constructed three fuel supply systems, one each for C_3H_8, natural gas, and H_2 systems.

A.   KEY ENABLING TECHNOLOGY

1.   Capstone C30 MicroTurbine

The C30 is an "adaptable, low-emission, and low maintenance power generation system" [14]. It is rated up to 30 kW. A single spool turbogenerator for electricity generation, it incorporates air bearings to reduce the frequency of maintenance required. A diagram of its typical engine is shown in Figure 14. This technology was chosen for its ability to "efficiently use a wide range of approved hydrocarbon-based gaseous and liquid fuels" [14]. This flexibility indicated capable technology and the potential for using H_2. The CRMS enabled remote operation, increasing safety during operation, and allowed data collection essential to this research.

This research used two C30 engines both rated for use with natural gas and C_3H_8, one with a high-pressure inlet and one with a low-pressure inlet. Commercial natural gas lines into buildings supply fuel at low pressures (between 1.72 and 34.5 kilopascals (kPa) depending on the location in the supply line). The C30 requires fuel from 350–380 kPa at the inlet [14]. The low-pressure C30 contains a booster pump to increase the fuel pressure if the supply pressure is too low. The high-pressure C30 contains no such pump and requires the fuel supply to be at an adequate pressure. The different C30s at the TPL provided flexibility in using different fuel supplies, including a low-pressure natural gas line and high-pressure cylinders of C_3H_8 and H_2.
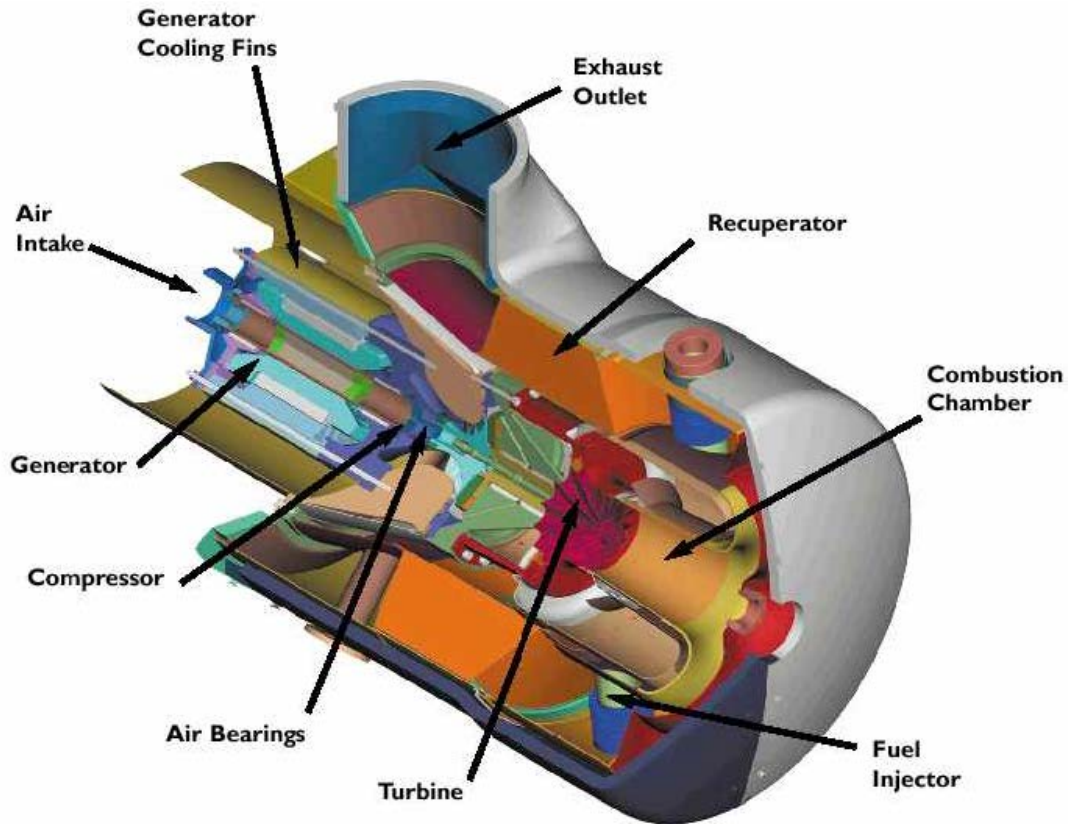
Figure 14.   Typical Capstone MicroTurbine Engine. Source: [14].

2.   Additional Components

Each fuel supply system required components suitable for use with each type of fuel. H_2 is more flammable than C_3H_8 or CH_4. The fuel supply system for H_2 required additional safety precautions in the form of component selections and procedures for operation. Components were selected on the basis of material properties (e.g., resistance to H_2 embrittlement) and availability at the TPL.

B. PROPANE-FUELED SYSTEM

The C_3H_8-fueled system connects a tank of C_3H_8 to the high-pressure C30 via a brass regulator and flexible hose tubing. These components are well-tested for C_3H_8 use. The high-pressure C30 was selected because the C_3H_8 tank supplies fuel at or above the specified pressure [14]. Figure 15 shows the tank, regulator, and flexible hose tubing.

Figure 15. C_3H_8 tank, regulator, and flexible tubing assembly

C. NATURAL GAS-FUELED SYSTEM

The natural gas-fueled system required the installation of a low-pressure natural gas line. Naval Facilities Engineering Command at NPS installed the natural gas line and connected it to the low-pressure C30. The line supplies natural gas at 34.5 kPa and has a manual shutoff valve 40 centimeters from the connection to the C30. It is stored in a shed for protection from the elements. A duct guides exhaust air from the C30 out of the shed, as in Figure 16.

Figure 16.   Low-pressure C30 inside the protective shed with the exhaust duct visible near the top of the image

D.   HYDROGEN-FUELED SYSTEM

The H_2-fueled system required the construction of a separate, H_2-rated fuel supply system to fuel the high-pressure C30. The high-pressure C30 was selected because the H_2 tank supplies H_2 at or above the specified pressure [14]. A H_2 tank leads to a regulator with inlet and outlet pressure gauges, a manual shutoff valve, a check valve, tubing, two solenoid valves, and a flame arrestor. The tubing, regulators, and valves used in the H_2 system are comprised of copper and stainless steel. The flame arrestor is brass. Figures 17 through 19 show the experimental setup.
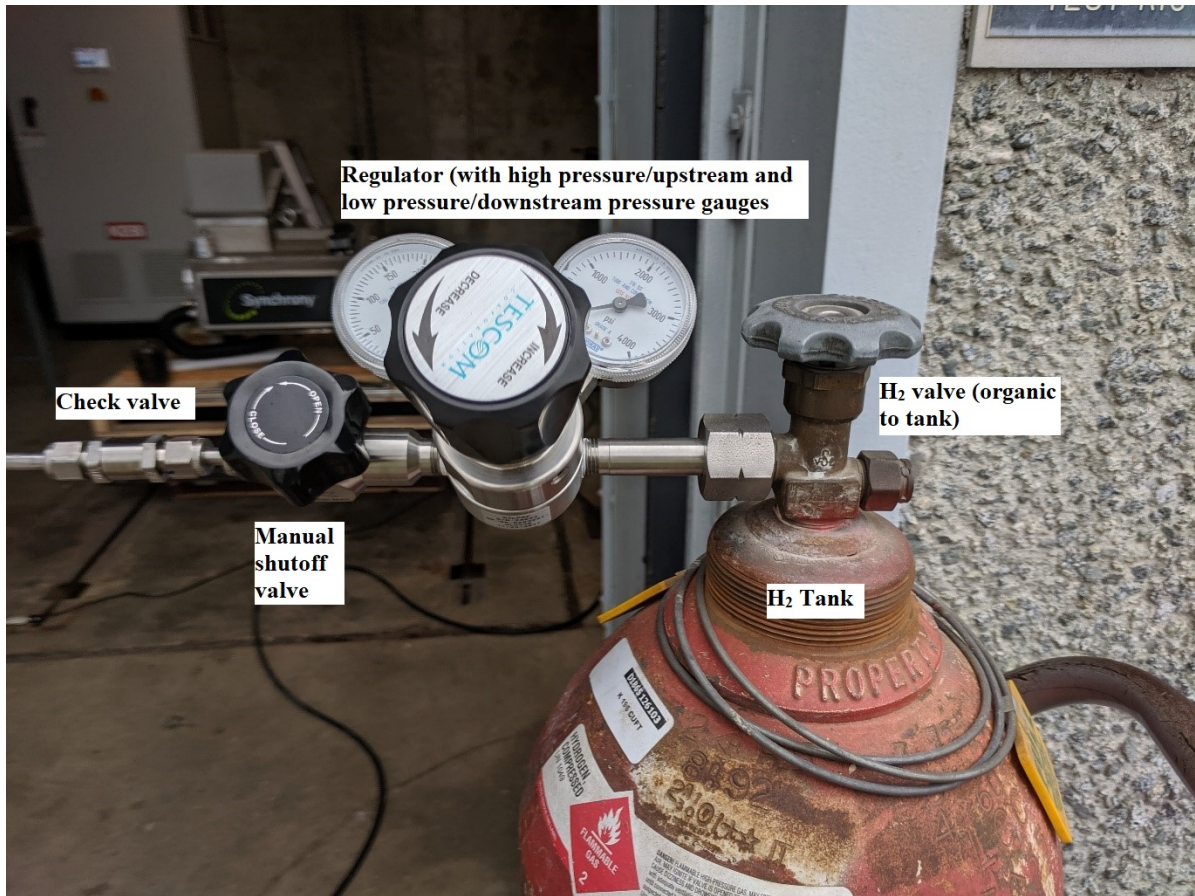
Figure 17. H_2 regulator assembly, including the regulator, pressure gauges, manual shutoff valve, and check valve

The H_2 tank is visible on the right side of Figure 17. The regulator, manual shutoff valve, and check valve are attached. The regulator, including the inlet and outlet pressure

valves, leads to the manual shutoff valve. A check valve is downstream of the shutoff valve to prevent flow towards the H_2 tank in the event of flashback. Stainless steel tubing connects the regulator assembly to the vertically mounted components, including two solenoid valves and the flame arrestor.

Figure 18 shows a section of the vertically mounted stainless steel tubing, connected to the flame arrestor and a solenoid valve. The flame arrestor comprises a heat sink and a one-way check valve that will extinguish a flame and prevent further propagation if one travels upstream ("flashback") towards a fuel source and an overpressure relief valve. The solenoid valves control H_2 flow into the engine or through a vent and are controlled remotely.
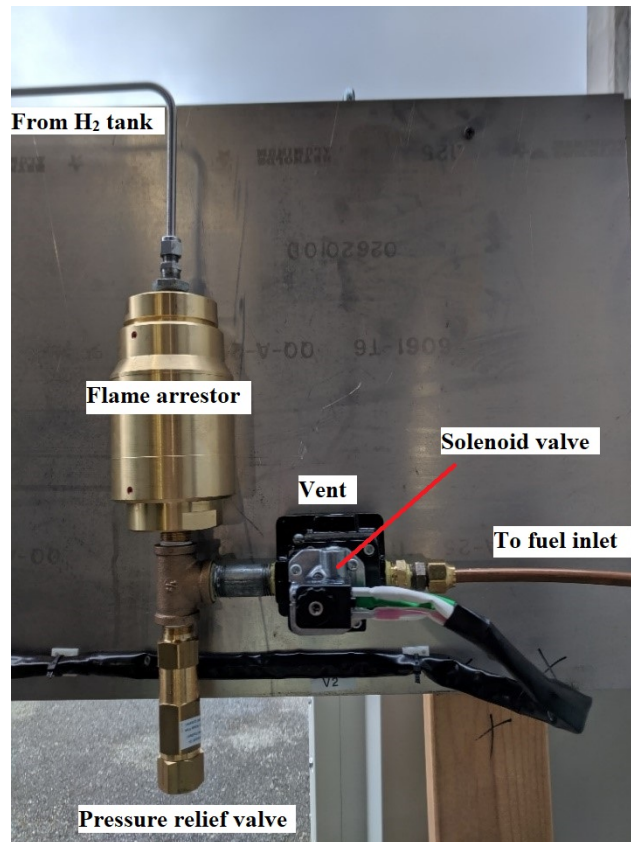
Figure 18.   Flame arrestor and solenoid valve, vertically mounted on a steel panel

Figure 19 shows the entire fuel supply system. The H_2 tank and the high-pressure C30 are connected to the system. The system was remotely controlled for safety. The procedure for operating the H_2 fuel supply system can be briefly described as manually opening the H_2 tank, evacuating the area, remotely actuating the solenoid valves, and remotely starting the C30. The procedure is described in detail in Appendix E.
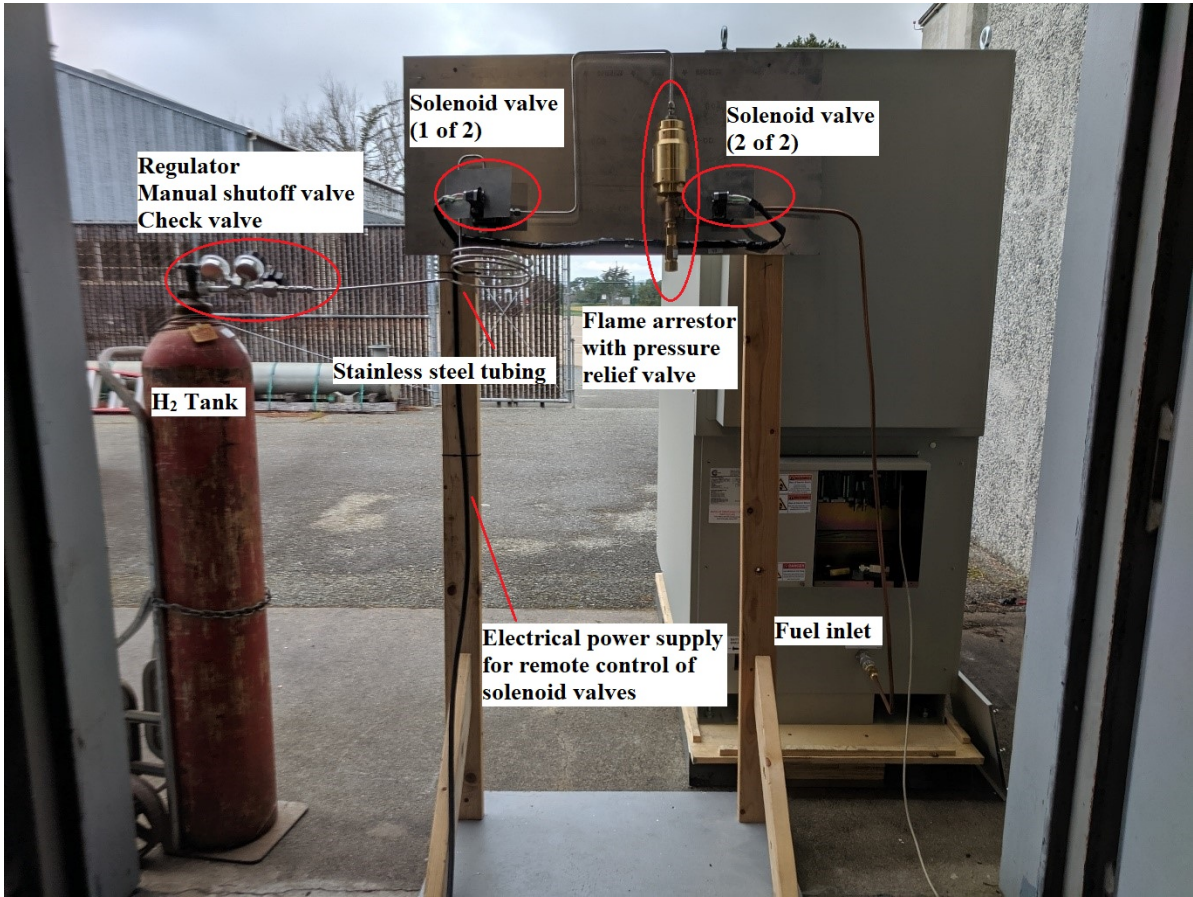
Figure 19.   Full H_2 fuel supply system

THIS PAGE INTENTIONALLY LEFT BLANK

IV. OPERATION OF CAPSTONE C30 MICROTURBINE

The Capstone Remote Monitoring System (CRMS) enabled the collection of detailed operational data from both C30s. The low-pressure C30 ran on natural gas; the high-pressure C30 ran on C_3H_8 and H_2. Operation times ranged from 1 minute, 28 seconds to 1 hour, 9 minutes, and 45 seconds. Table 2 summarizes the data. A primary method of measuring whether combustion occurred and achieved steady-state operation inside the C30 is the turbine exit temperature (TET). The TET should rise quickly and then stabilize.

For all test runs, the start command was given by the user via the control mode in CRMS. C_3H_8 and natural gas test runs were shut down by a user command. The three H_2 runs shut down automatically in accordance with the C30's operating software with a fault code of 6012 ("FLAMEOUT_LOAD") [15].

A. RESULTS

Table 2 describes the pressure, duration of run, and temperature data collected from four test runs of the high-pressure C30 with C_3H_8 and H_2 and one test run of the low-pressure C30 with natural gas. Maximum TET and the change in TET (the initial TET subtracted from the maximum TET achieved) are both included in Table 2. The change in TET is included because the C30 was not cooled to ambient temperatures between H_2 runs. Complete cooling was time-prohibitive during testing; the raised initial temperature did not affect operation.

In addition to the quantitative data collected, qualitative observations of the sound produced by the C30 during operation indicates that natural gas has the smoothest operation. Operation with C_3H_8 produced a throbbing sound representative of an unstable flame inside the combustion chamber. The C30 was run at idle speeds, producing only the power required to charge the internal battery. Producing power may stabilize the C_3H_8 flame. The internal battery provides power at startup, bringing the turbine speed to 25000 revolutions per minute (RPM) prior to ignition. Initial operation with H_2 produced sounds akin to operation with natural gas: the C30 engine speed and sound correlated at startup and H_2 produced an audible "pop" sound at ignition. Although the flameout was not

audible, the slowing turbine could be heard following the fault code and automatic shutdown process.

Table 2.   Runtime data for C30 tests

Fuel	C_3H_8	Natural Gas	H_2 Run 1	H_2 Run 2	H_2 Run 3
Input Pressure [kPa]	414	34.5	276	448	517
Fuel Valve Exit Pressure [kPa]	409	310	35.2	51.0	53.8
$(TET_{maximum} - TET_{initial})$ [ºC]	625	636	189	399	429
Maximum TET [ºC]	676	674	235	517	604
Total Runtime [HH:MM:SS]	01:09:45	00:34:14	00:01:28	00:01:31	00:01:33
Time to Achieve 95% of Maximum TET [s]	18	22	15	15	17

1.   Propane-Fueled Operation, High-Pressure C30, Run 1 of 1

Figure 20 displays the engine speed profile for the entire duration of the test. The maximum engine speed achieved was 45338 RPM. Figure 21 displays the TET profile. The C30 operated for an extended period of time at steady-state. The sudden drop in TET visible in Figure 21 occurs when combustion is extinguished; air flow through the C30 continues as the compressor and turbine slow. The brief spike in TET in the final seconds of operation occur when the compressor and turbine have stopped the cooling airflow.

Figure 20.   Total runtime vs. engine speed (C_3H_8-fueled operation
with high-pressure C30)
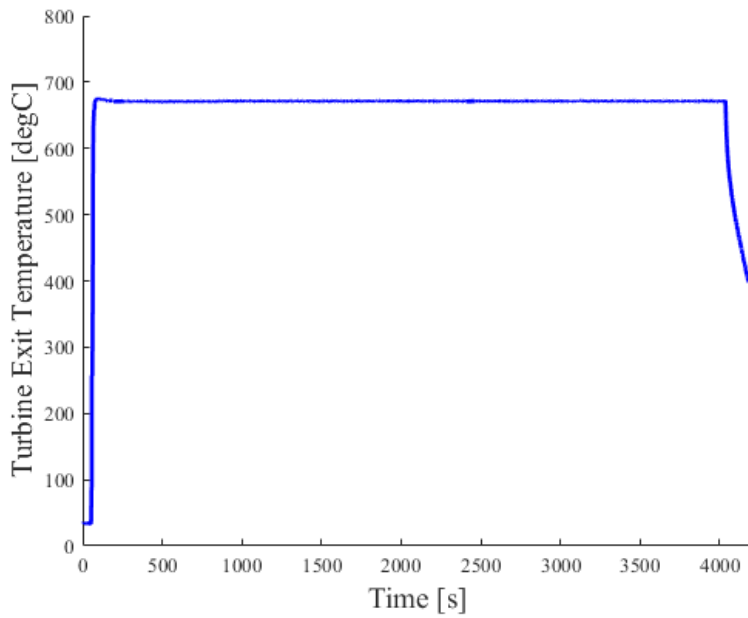
Figure 21.   Total runtime vs. turbine exit temperature (C_3H_8-fueled
operation with high-pressure C30)

2. Natural Gas (CH₄)-Fueled Operation, Low-Pressure C30, Run 1 of 1

Figure 22 displays the engine speed profile for the entire duration of the test. The maximum engine speed achieved was 51674 revolutions per minute (RPM). Figure 23 displays the TET profile. The C30 operated for an extended period of time at steady-state. During shutdown, the C30 will continue to operate to recharge the battery if its charge is less than 90% [14]. The "step" decrease in engine speed observed during the shutdown process, more visible than in the C_3H_8 run, is the result of this process. The C_3H_8 run operated for 1 hour, 9 minutes, and 45 seconds and charged the internal battery for more time than the natural gas run, which operated for 34 minutes and 14 seconds.

Figure 22.   Total runtime vs. engine speed (natural gas (CH₄)-fueled operation with low-pressure C30)
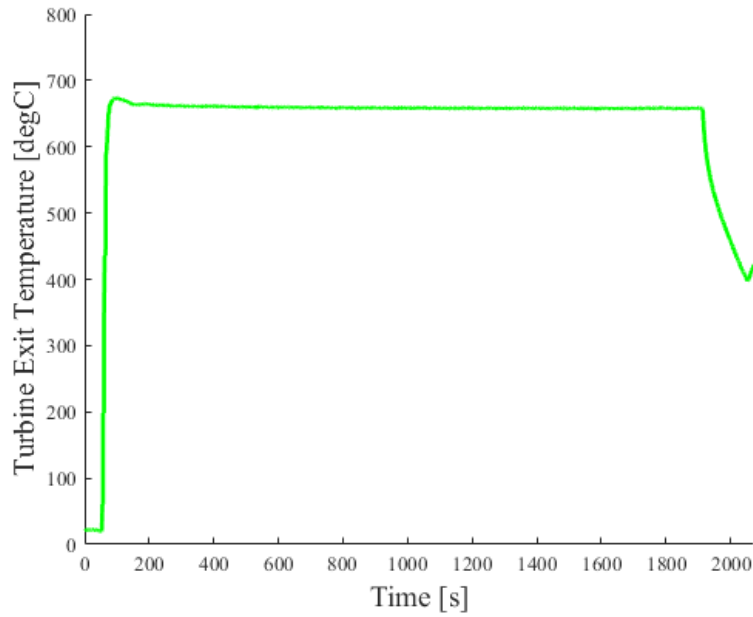
Figure 23.   Total runtime vs. turbine exit temperature (natural gas
(CH$_4$)-fueled operation with low-pressure C30)

3.   Hydrogen-Fueled Operation, High-Pressure C30, Run 1 of 3

Figure 24 displays the engine speed profile for the entire duration of the test. The maximum engine speed achieved was 46218 revolutions per minute (RPM). Figure 25 displays the TET profile. Ignition occurred at 53 s. The C30 operated for a short period of time and did not achieve steady-state.
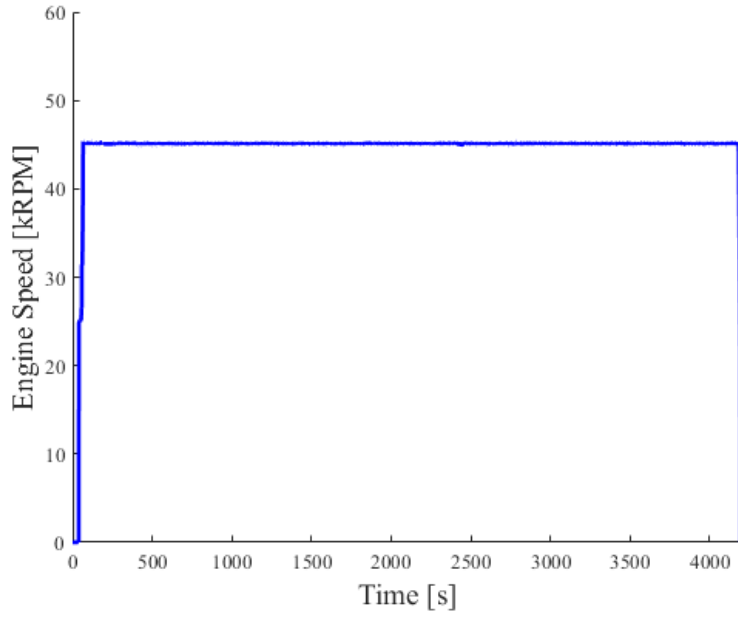
Figure 24. Total runtime vs. engine speed (H₂-fueled operation with high-pressure C30, Run 1)
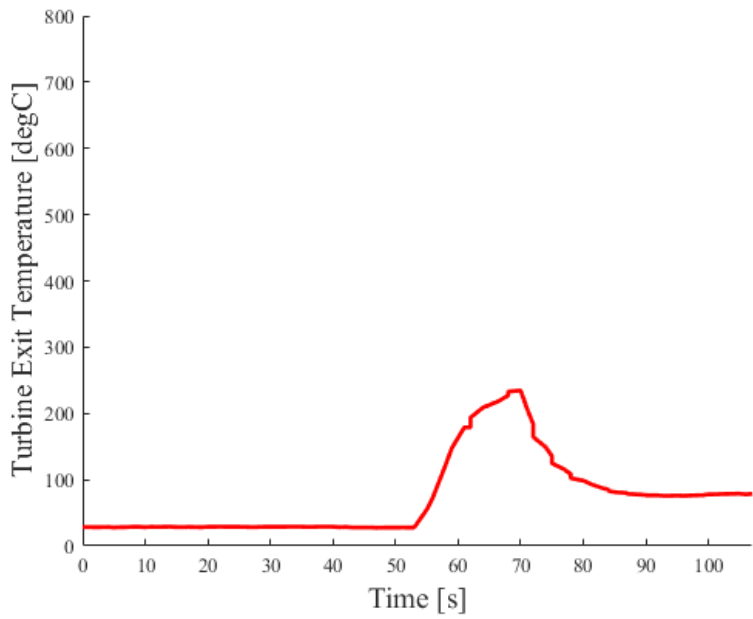
Figure 25. Total runtime vs. turbine exit temperature (H₂-fueled operation with high-pressure C30, Run 1)

36

4. Hydrogen-Fueled Operation, High-Pressure C30, Run 2 of 3

Figure 26 displays the engine speed profile for the entire duration of the test. The maximum engine speed achieved was 45636 revolutions per minute (RPM). Figure 27 displays the TET profile. Ignition occurred at 53 s. The C30 operated for a short period of time and did not achieve steady-state.
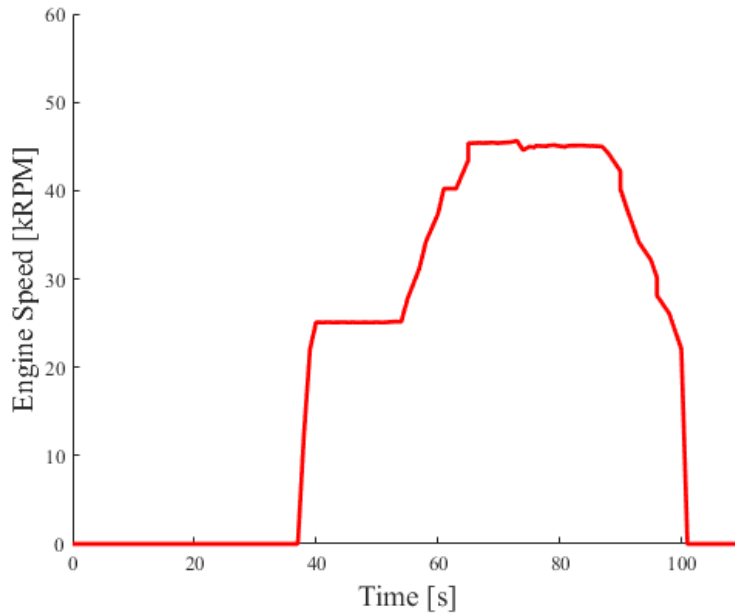
Figure 26.   Total runtime vs. engine speed (H_2-fueled operation with high-pressure C30, Run 2)
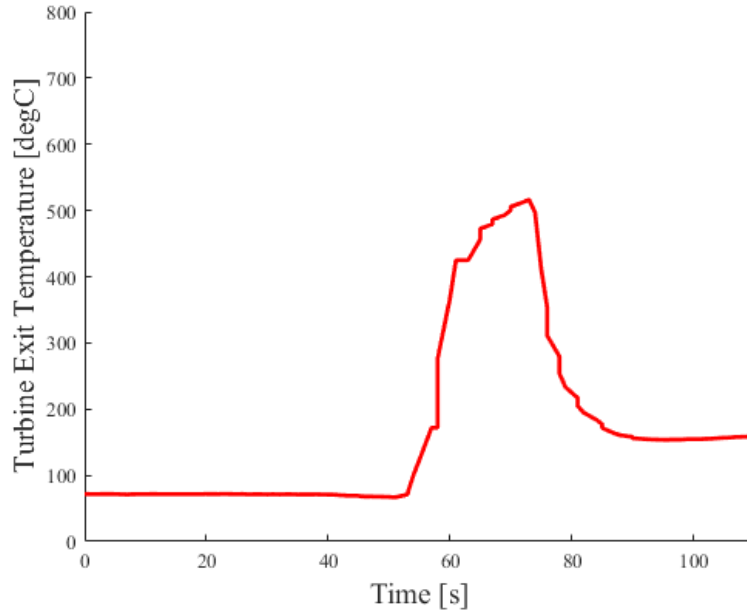
Figure 27.   Total runtime vs. turbine exit temperature (H_2-fueled
operation with high-pressure C30, Run 2)

5.   **Hydrogen-Fueled Operation, High-Pressure C30, Run 3 of 3**

Figure 28 displays the engine speed profile for the entire duration of the test. The maximum engine speed achieved was 45402 revolutions per minute (RPM). Figure 29 displays the TET profile. Ignition occurred at 53 s. The C30 operated for a short period of time and did not achieve steady-state.
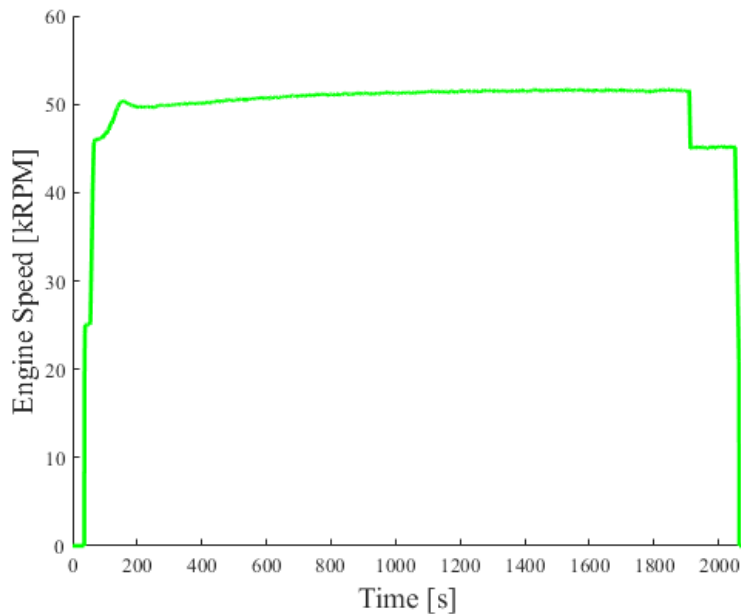
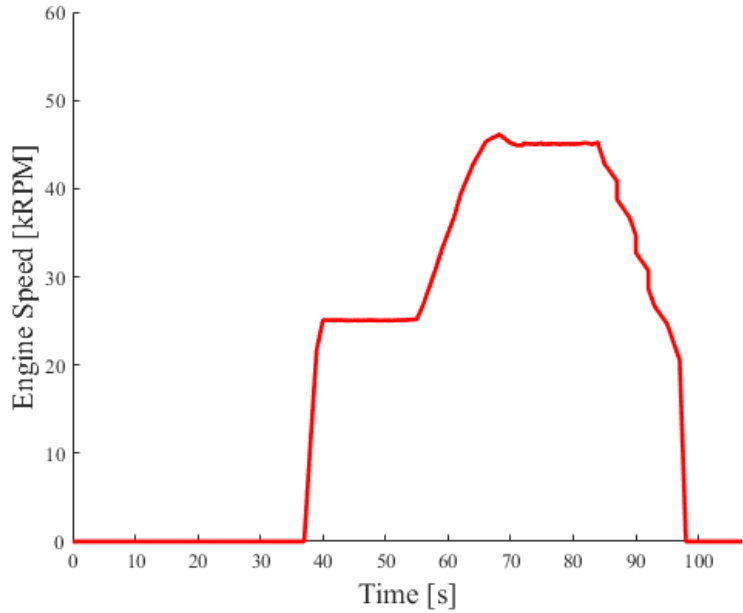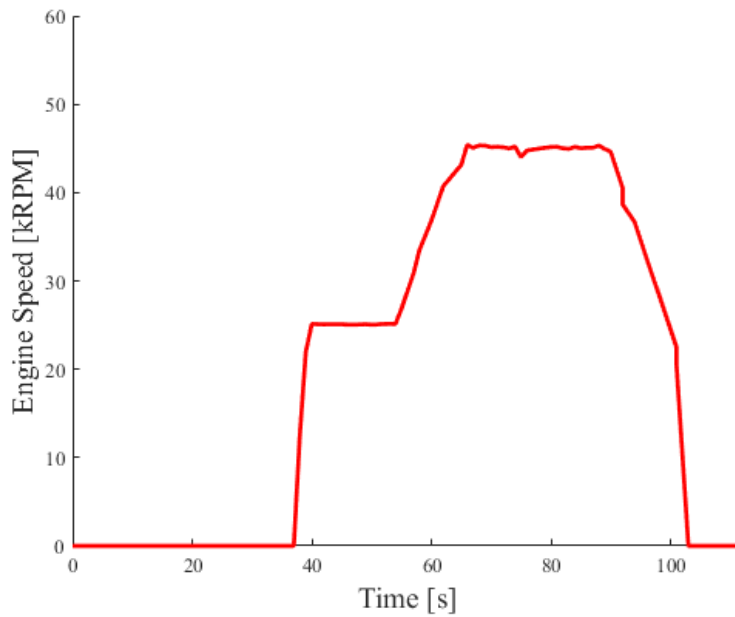Figure 28.   Total runtime vs. engine speed (H$_2$-fueled operation with high-pressure C30, Run 3)
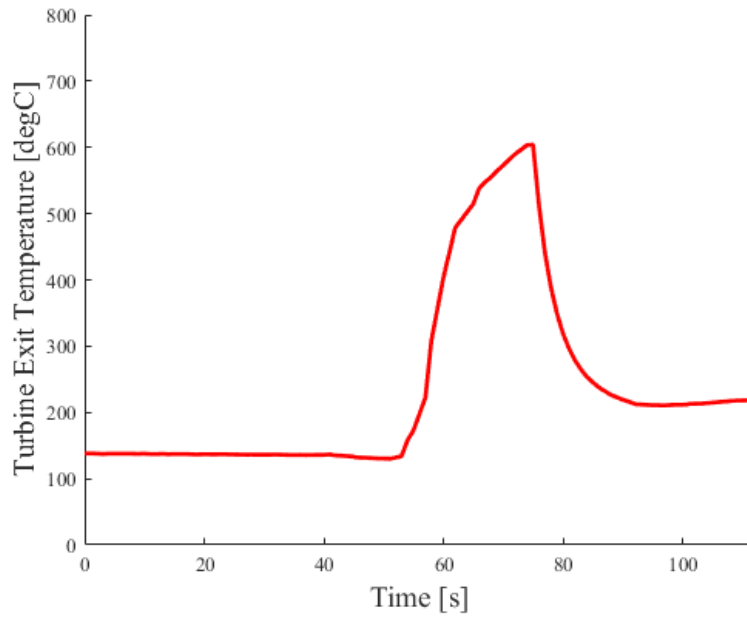
Figure 29.   Total runtime vs. turbine exit temperature (H$_2$-fueled operation with high-pressure C30, Run 3)

B.   ANALYSIS

The engine speed and TET profiles of C_3H_8, natural gas, and H_2 combustion trend together at startup (from the time at which the C30's internal fuel valve opens to the time at which 95% of the maximum TET for each run is achieved) as shown in Figures 30 and 31. These trends indicate that the C30 combusts the three fuels similarly. Appendix F contains calculations of the mass energy density and volumetric energy density of the fuels used at the temperatures and pressures used in the fuel supply systems. The similarity of the final TET, despite the differences in fuel energy densities, indicates that TET is a programmed set point within the C30.
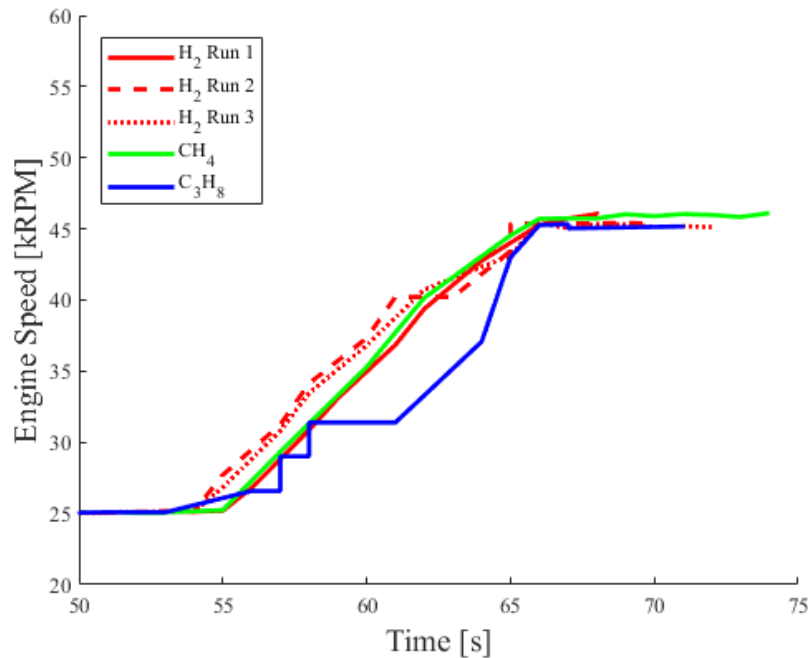
Figure 30.   Engine speed from start command to time at which 95% of maximum TET is achieved
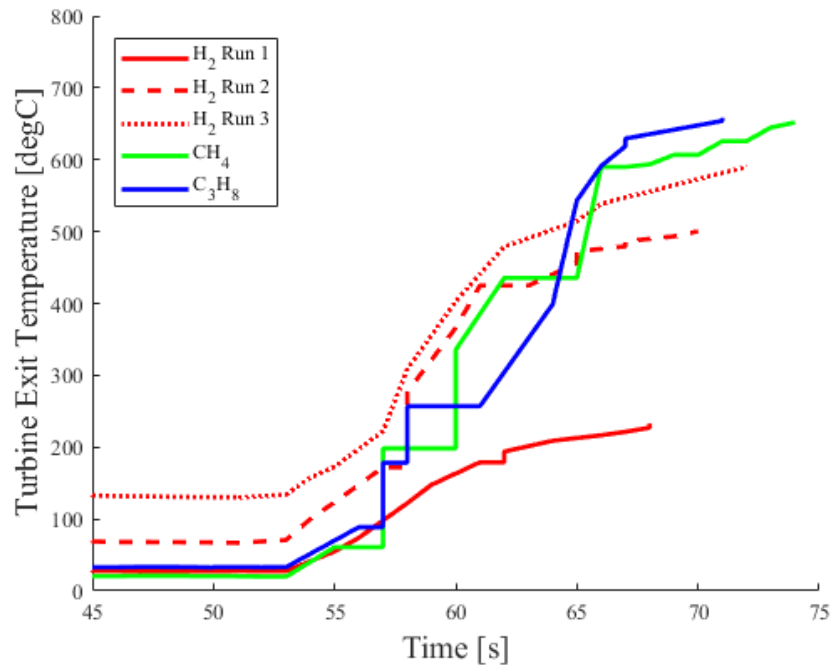
Figure 31.   TET from start command to time at which 95% of
maximum TET is achieved

C$_3$H$_8$ and natural gas operated at steady-state, maintaining constant speed and temperature on the timescale of minutes to hours. H$_2$ operated for approximately 1 minute and 30 seconds for each of the three test runs; each caused the C30 to stop automatically in accordance with its programming due to a fault code 6012 ("FLAMEOUT_LOAD") [15]. The cause of the flameout is predicted to be a lean blowout. The insufficient volumetric H$_2$ flow coupled with the fast laminar flame speed of H$_2$ could not sustain combustion. Increasing the fuel supply pressure and therefore the fuel supply velocity and volumetric flow rate increased the runtime for the three runs. Figure 32 plots the total runtime against the fuel system supply pressure. The text describes the pressure data at the C30's internal fuel valve outlet collected from CRMS. This is lower than the actual fuel supply pressure due to pressure losses in a real system.
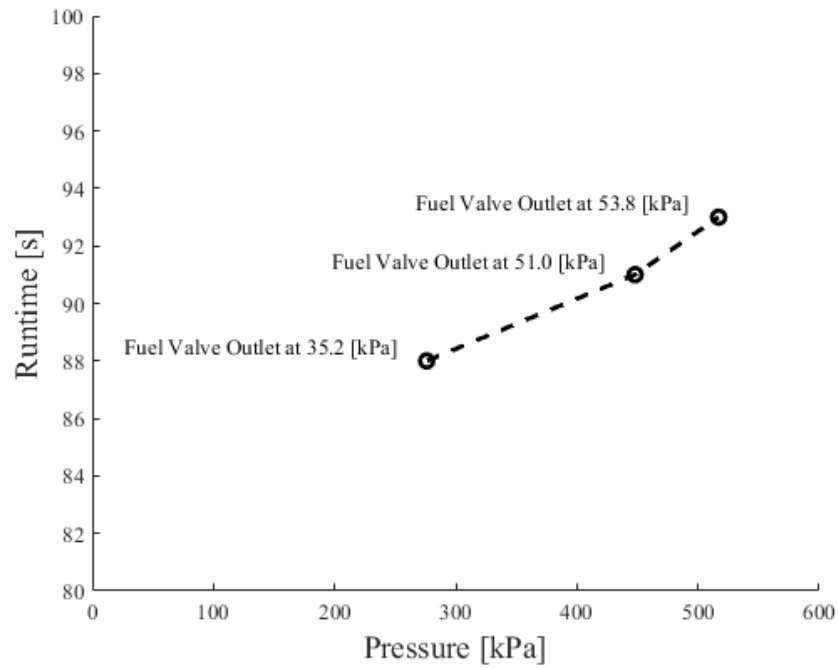
Figure 32.   Effect of increasing fuel supply pressure on the duration of
H_2 operation

As the H_2 supply pressure increased measured at the regulator, the fuel valve outlet pressure did not increase proportionally. The internal fuel supply system is predicted to have choked the flow, preventing higher pressures, velocities, and volumetric flow rates necessary to sustain combustion in the C30. This concern is readdressed in the Recommendations section of Chapter V.

V.   CONCLUSION AND FUTURE WORK

This thesis set out to operate a COTS microturbine on H_2. This goal was achieved, albeit for a short period of time. This research approached the challenges of increasing energy resilience using H_2 using the Capstone C30 MicroTurbine. Following baseline testing with natural gas and C_3H_8, a H_2 fuel supply system was designed, developed, and implemented. The CRMS aided data collection and enabled safe remote operation of the C30. This research demonstrated that a COTS microturbine can operate using H_2, indicating its role in a larger hydrogen energy storage and generation system and a future hydrogen economy.

A.   DISCUSSION OF RESULTS

In conclusion, the C30 demonstrates an ability to operate on H_2 instead of light hydrocarbons such as natural gas or C_3H_8. Figures 30 and 31 show that the C30 starts up with H_2 following the same procedure and trends as with natural gas and C_3H_8. However, combustion was not sustained. Each of three test runs caused a fault and automatic shutdown in succession. The TET rose with each test run, culminating on the third run with a TET comparable in magnitude to the steady-state operating TET of natural gas and C_3H_8. Due to the short runtimes, the steady-state operating TET of H_2 is not known; however, it is predicted to be very similar to natural gas and C_3H_8 because the TET and engine speed are set operating parameters within the C30 based on load.

B.   RECOMMENDATIONS

Following the results of the CFD simulations, analysis of the materials used in the C30's combustion chamber is strongly recommended. Although the TET appears to be a set point, the temperature inside the combustion chamber is not measured and the effects of combusting H_2 within it are unknown. Any effects did not preclude the C30 from operating normally using C_3H_8 six days after the H_2 test runs.

The H_2 fuel supply system should be redesigned to provide greater volumetric flow rates and the ability to control the flow rate. The design may be a limiting factor in the

operation of the C30 during this research. Other limiting factors include the design of the internal fuel supply system within the C30 causing choked flow or the fuel nozzle design inside the combustion chamber.

Incorporating a resistor bank to test the C30 at full power is strongly recommended. The increased fuel demand may stabilize the flame in the combustion chamber, especially for operation with C_3H_8.

C. FUTURE WORK

The next stage of this research should first incorporate a resistor bank to test the C30 at full power and compare results to this research. Next, future work might focus on constructing an improved H_2 fuel supply system, capable of greater volumetric flow rates and containing more instrumentation in the form of flow meters, pressure gauges, and thermocouples or focus on improving the internal design of the C30's fuel nozzles and combustion chamber. Instrumentation could be added to the combustion chamber or combustion chamber outlet of the C30, especially if changing components within the chamber. Collecting data from the combustion chamber while operating with H_2 at steady-state operation would provide more information to improve the technology of a future hydrogen economy.

APPENDIX A. FUEL INLET VELOCITY CALCULATION

For an inversely proportional relationship between fuel inlet velocity and mass air-fuel ratio, it can be shown that:

$$MAF = \frac{k}{v}$$

Where v is the fuel inlet velocity, k is a constant, and MAF is the mass air-fuel ratio. Substituting simulation values for v and MAF and averaging the calculated k values:

$$k = 11300$$

Calculating the mass air-fuel ratio twice that of the stoichiometric mass air-fuel ratio for H_2 [12]:

$$MAF = 2 \times \Phi_{H_2} = 2 \times 34.3 = 68.6$$

Substituting and calculating for v:

$$v = \frac{k}{MAF} = \frac{11300}{68.6} = 165 \left[\frac{m}{s}\right]$$

THIS PAGE INTENTIONALLY LEFT BLANK

APPENDIX B. CFD COMBUSTION SIMULATION DATA

A.   PROPANE-AIR COMBUSTION

Fuel Inlet Velocity [m/s]	Maximum Temperature [K]	Fuel Mass Flow Rate [kg/s]	Air Mass Flow Rate [kg/s]	Secondary Air Mass Flow Rate [kg/s]	Air-Fuel Mass Flow Ratio [-]	Equivalence Ratio [-]
40	2392.49	0.0059932	0.0689049	0.00845221	12.90748	0.8237

B.   METHANE-AIR COMBUSTION

Fuel Inlet Velocity [m/s]	Maximum Temperature [K]	Fuel Mass Flow Rate [kg/s]	Air Mass Flow Rate [kg/s]	Secondary Air Mass Flow Rate [kg/s]	Air-Fuel Mass Flow Ratio [-]	Equivalence Ratio [-]
40	2225.44	0.00218032	0.0688703	0.00844901	35.46	2.063

C.   HYDROGEN-AIR COMBUSTION

Fuel Inlet Velocity [m/s]	Maximum Temperature [K]	Fuel Mass Flow Rate [kg/s]	Air Mass Flow Rate [kg/s]	Secondary Air Mass Flow Rate [kg/s]	Air-Fuel Mass Flow Ratio [-]	Equivalence Ratio [-]
10	1998.89	6.85E-05	0.0688229	0.0084451	1128	32.88
15	1998.97	0.000102758	0.0688248	0.008844523	755.9	22.04
20	2046.59	0.000137013	0.0688269	0.008844536	566.9	16.53
25	1998.45	0.00017127	0.0688289	0.00844549	451.2	13.15
30	206256	0.000205526	0.0688309	0.00844563	376.0	10.96
35	2095.34	0.000239783	0.0688331	0.00844578	322.3	9.396
40	2151.32	0.00027404	0.0688353	0.00844593	282.0	8.222
45	2135.68	0.000308296	0.0688375	0.00844609	250.7	7.308

Fuel Inlet Velocity [m/s]	Maximum Temperature [K]	Fuel Mass Flow Rate [kg/s]	Air Mass Flow Rate [kg/s]	Secondary Air Mass Flow Rate [kg/s]	Air-Fuel Mass Flow Ratio [-]	Equivalence Ratio [-]
50	2174.83	0.000342552	0.0688398	0.00844625	225.6	6.578
55	2211.87	0.000376807	0.0688422	0.00844642	205.1	5.980
60	2247.90	0.000411061	0.0688444	0.008844658	189.0	5.510
165	2491.92	0.00113019	0.0688847	0.00844978	68.43	1.995

APPENDIX C. CFD COMBUSTION SIMULATION IMAGE

ANSYS CFX produces temperature scales from the minimum to the maximum temperatures calculated. The scales, visible in on the left-hand side of each figure, vary with each scenario.

A. PROPANE-AIR COMBUSTION
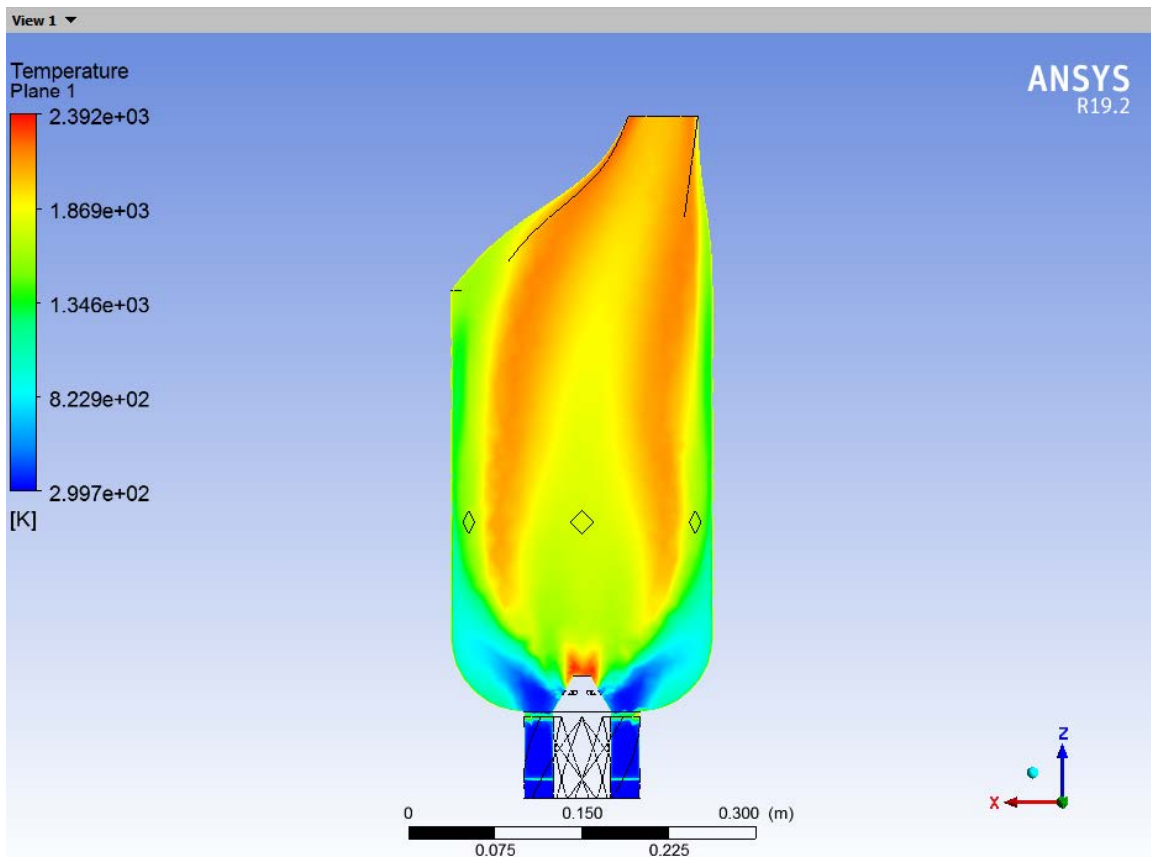
Temperature inside the combustion chamber (propane-air reaction, 40 m/s)

B.   METHANE-AIR COMBUSTION
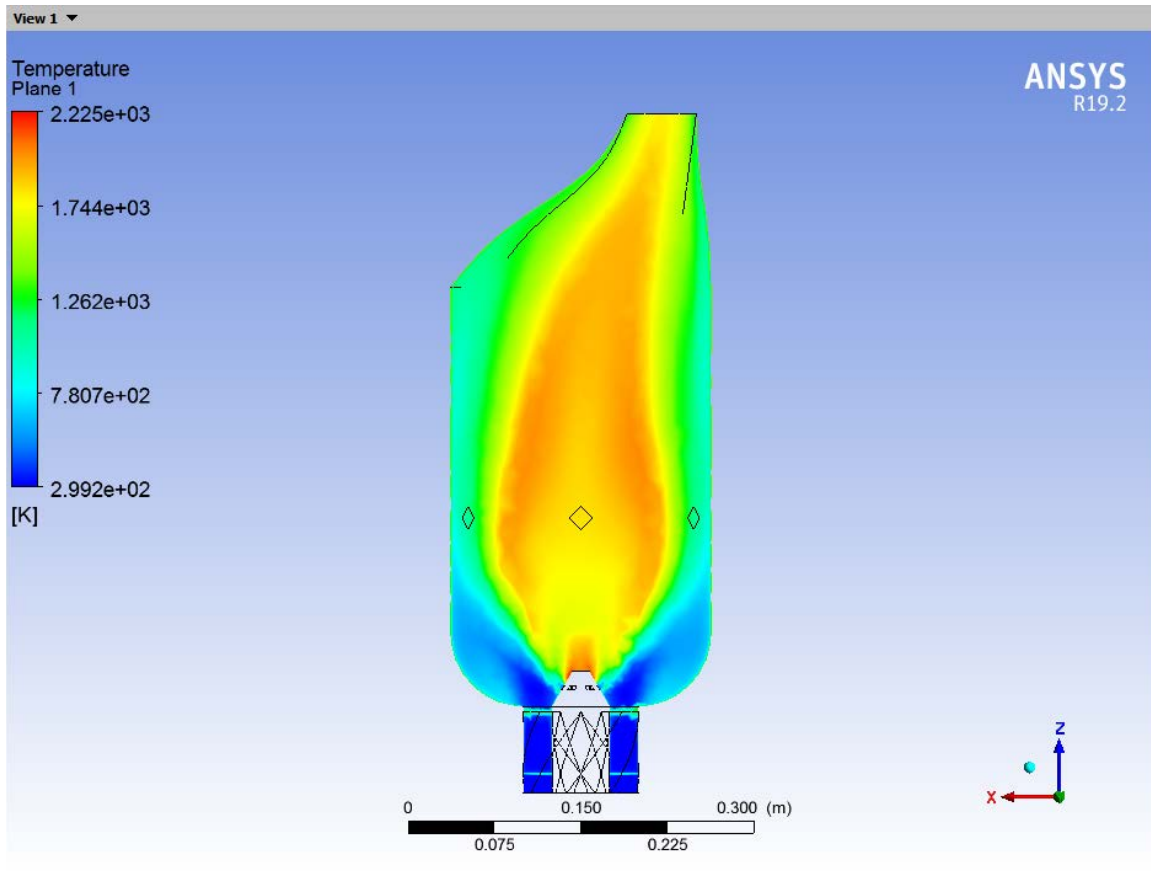
Temperature inside the combustion chamber (methane-air reaction, 40 m/s)

C. HYDROGEN-AIR COMBUSTION
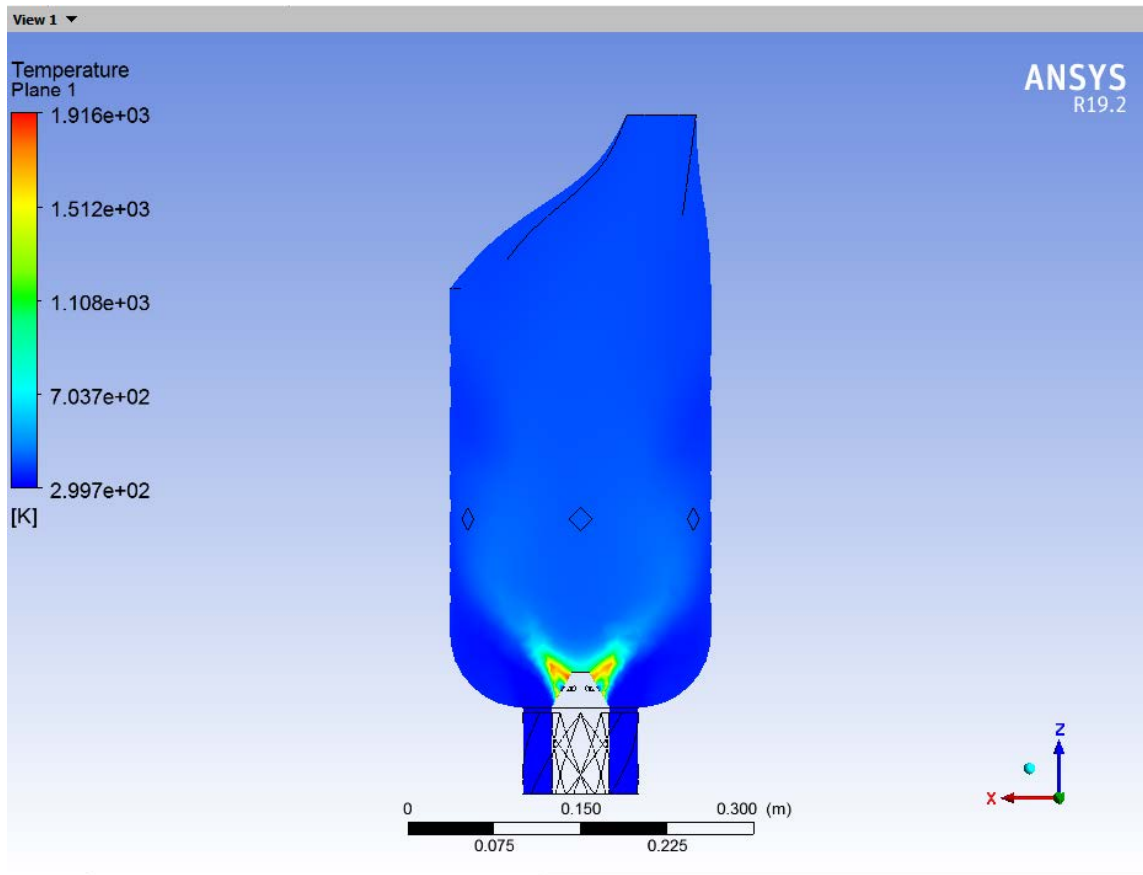
Temperature inside the combustion chamber (H_2-air reaction, inlet velocity 10 m/s)
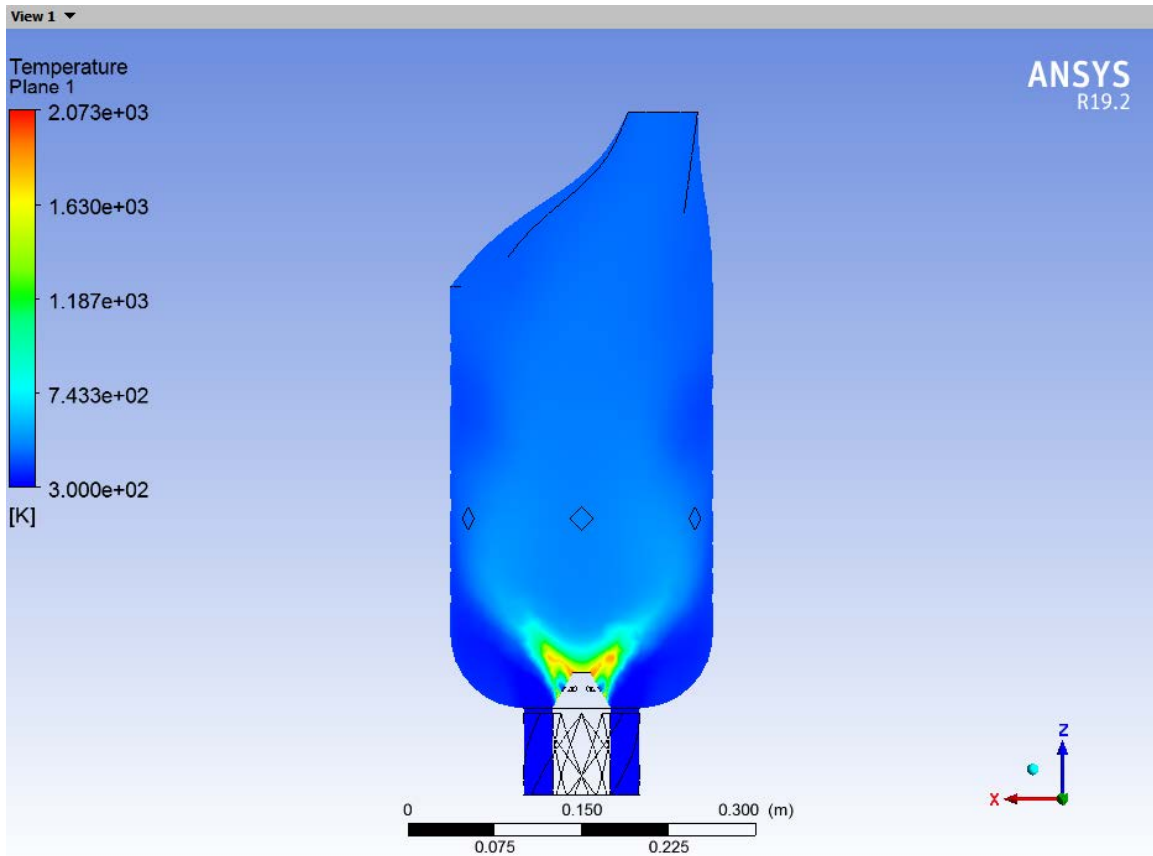
Temperature inside the combustion chamber (H_2-air reaction, inlet velocity 15 m/s)
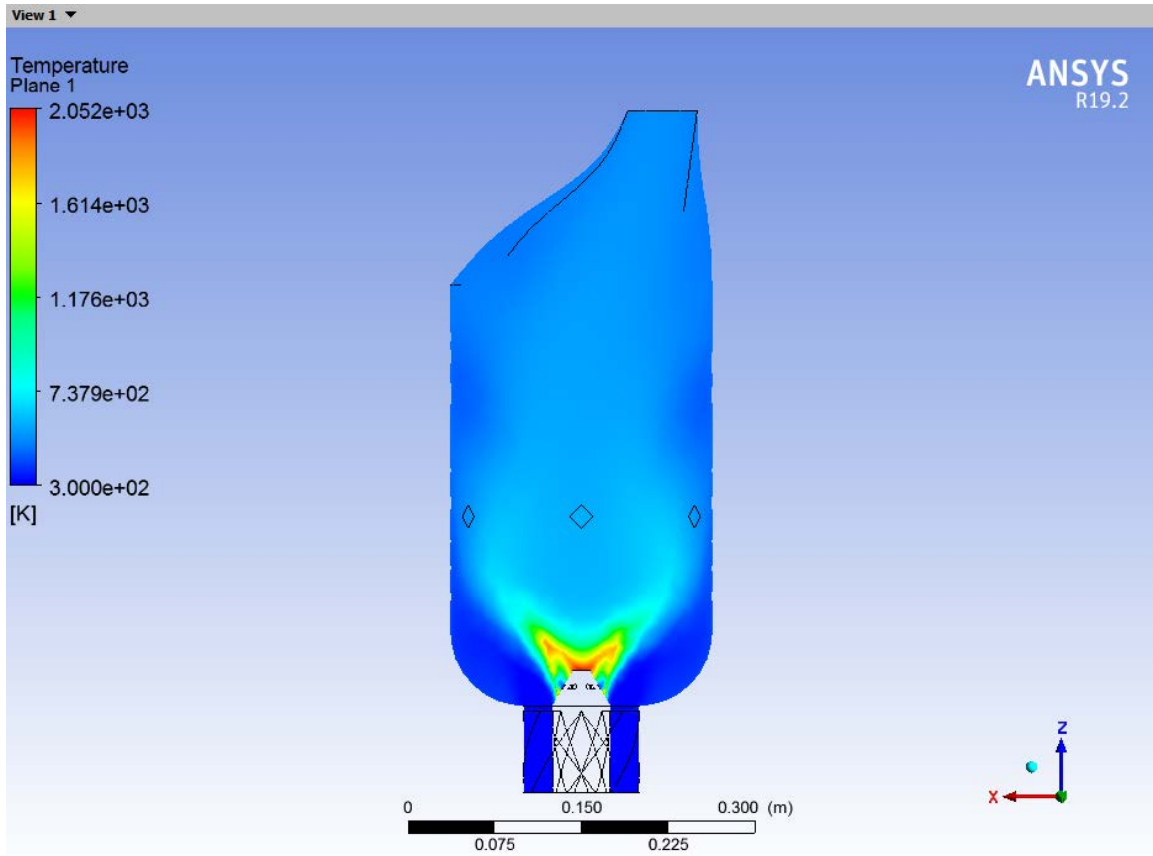
Temperature inside the combustion chamber (H$_2$-air reaction, inlet velocity 20 m/s)
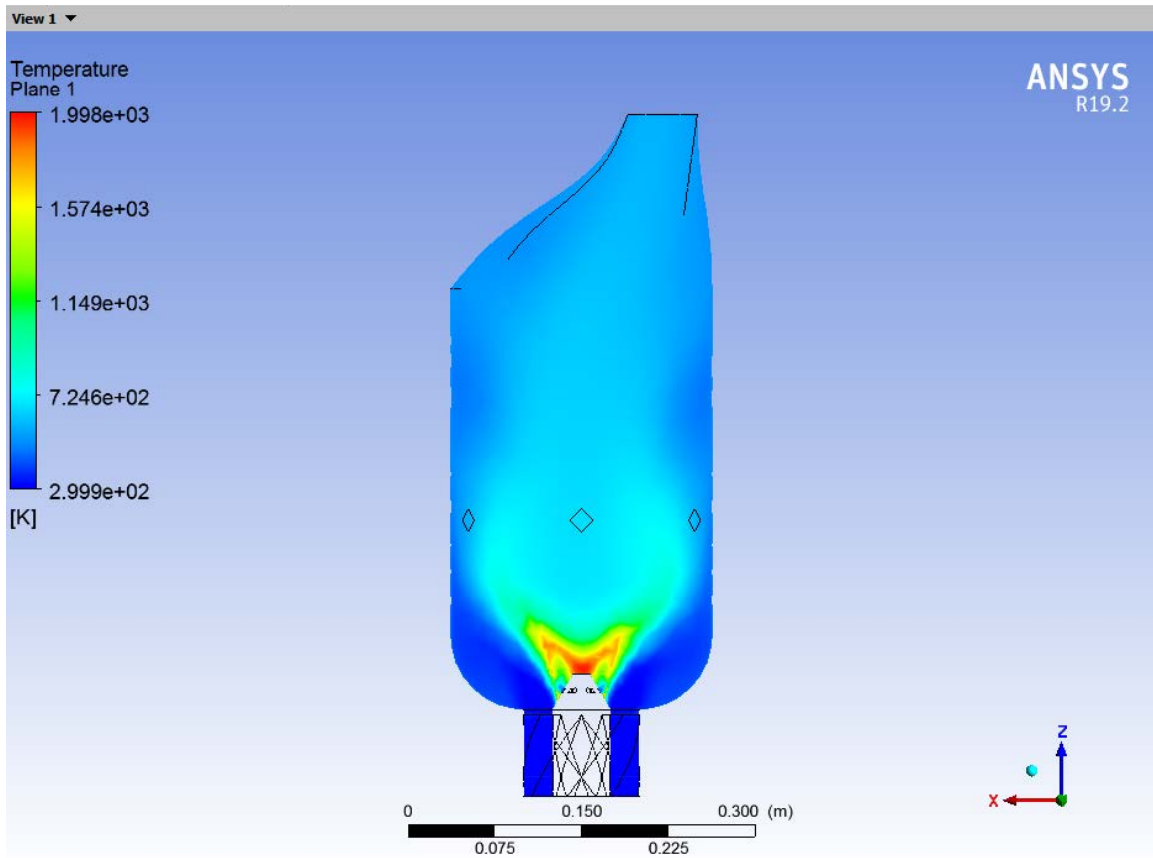
Temperature inside the combustion chamber (H$_2$-air reaction, inlet velocity 25 m/s)
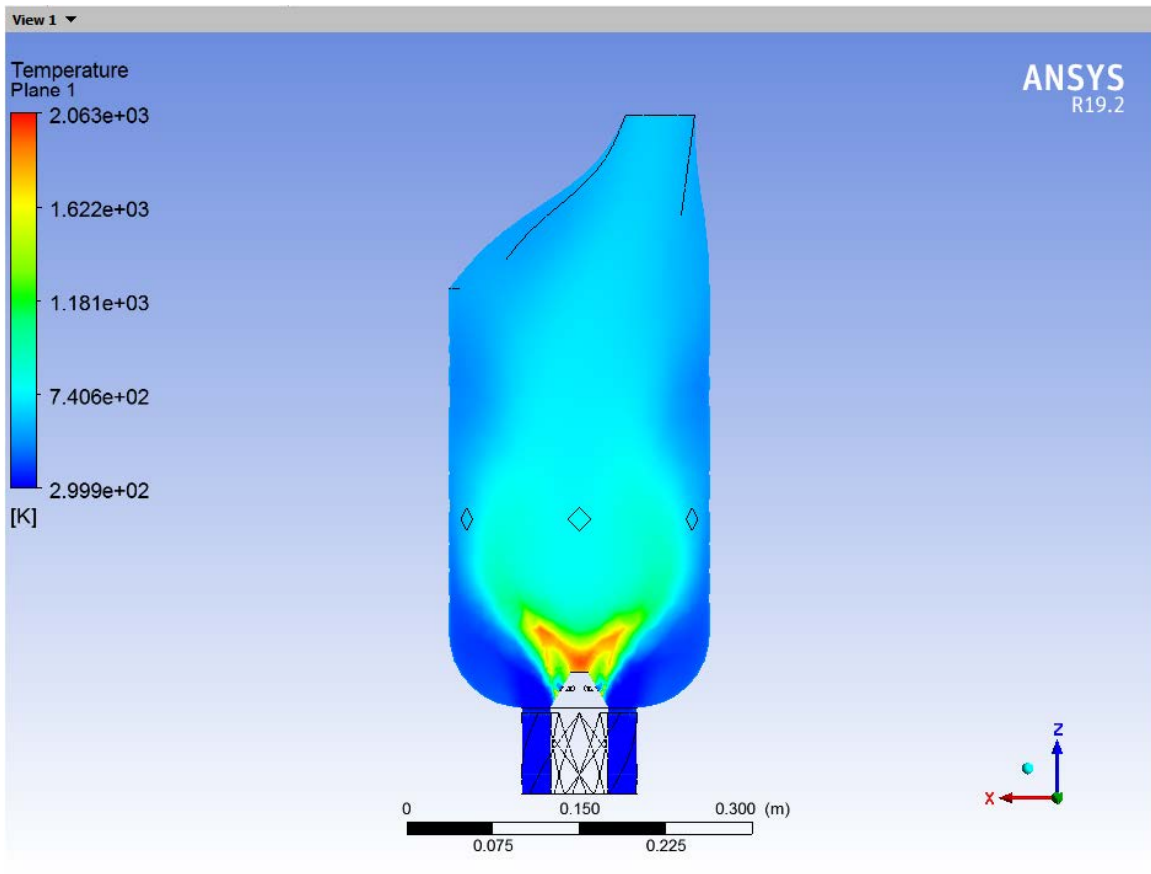
Temperature inside the combustion chamber (H$_2$-air reaction, inlet velocity 30 m/s)
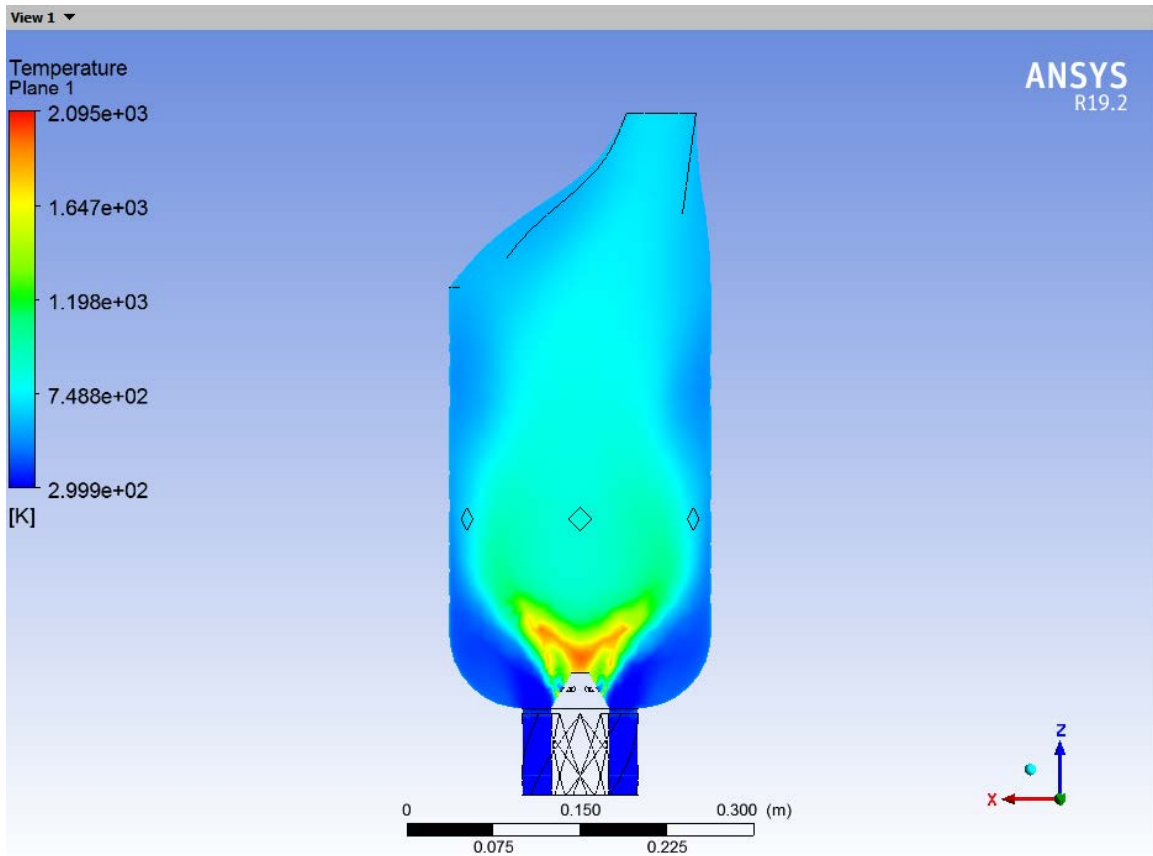
Temperature inside the combustion chamber (H$_2$-air reaction, inlet velocity 35 m/s)
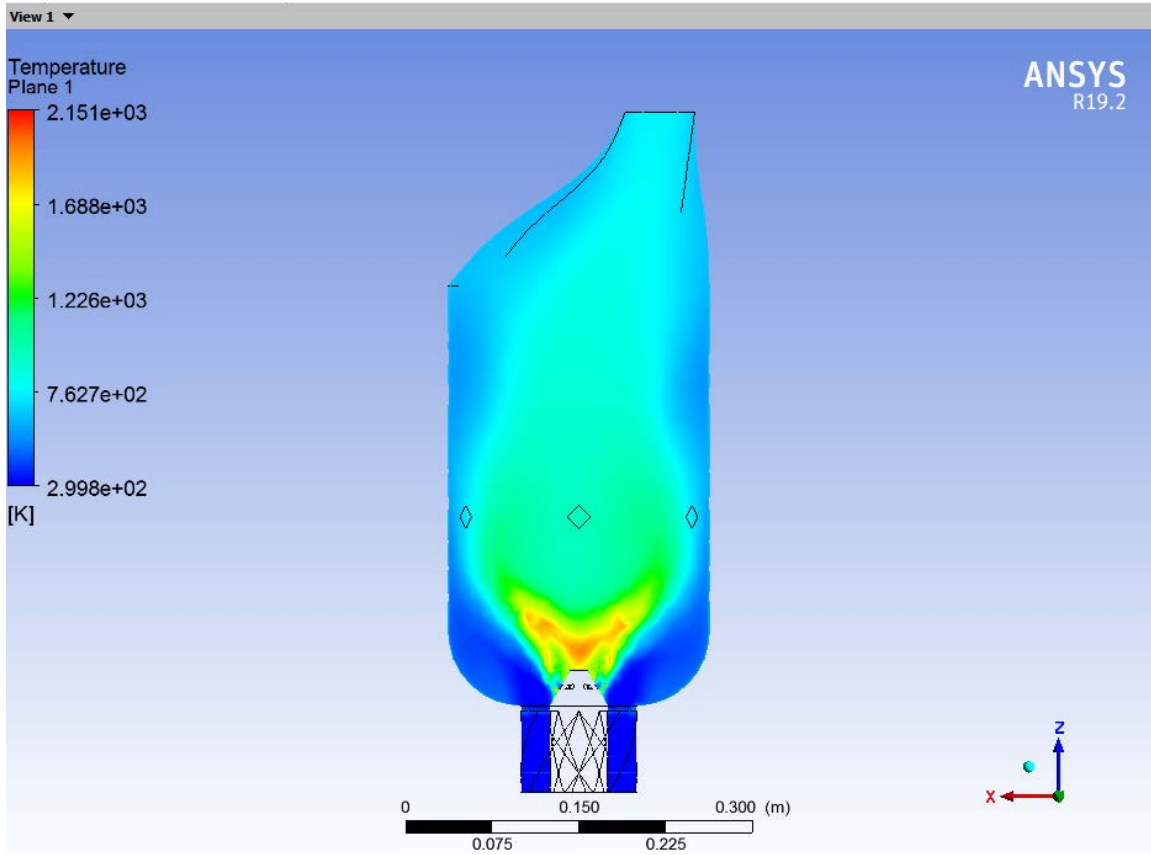
Temperature inside the combustion chamber (H_2-air reaction, inlet velocity 40 m/s)
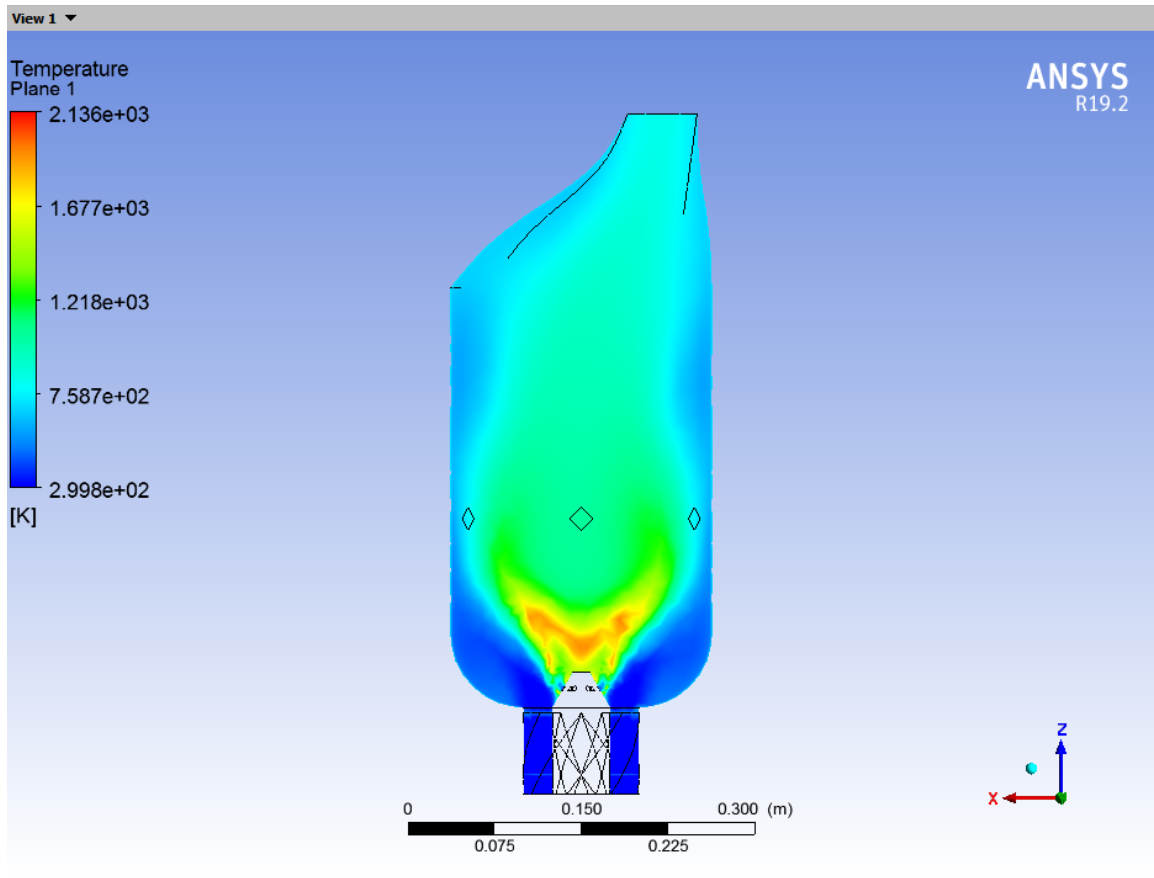
Temperature inside the combustion chamber (H_2-air reaction, inlet velocity 45 m/s)
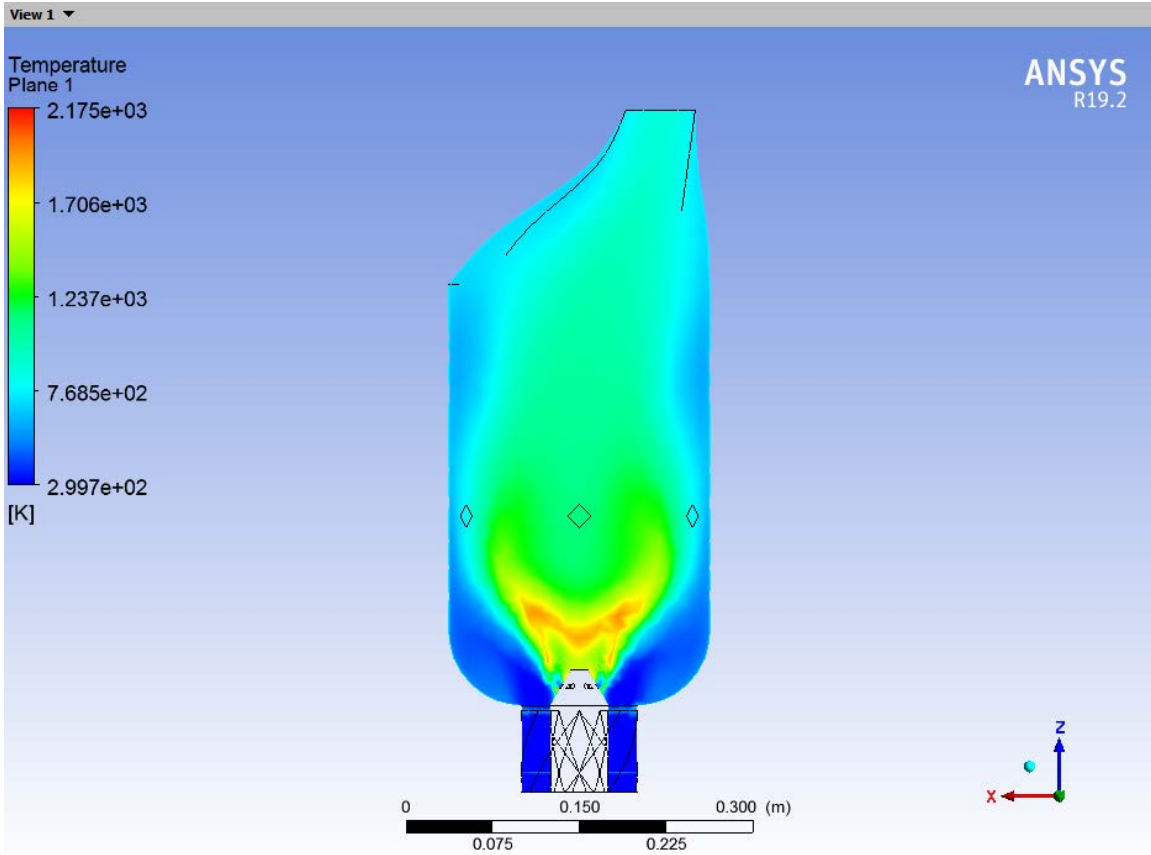
Temperature inside the combustion chamber (H$_2$-air reaction, inlet velocity 50 m/s)
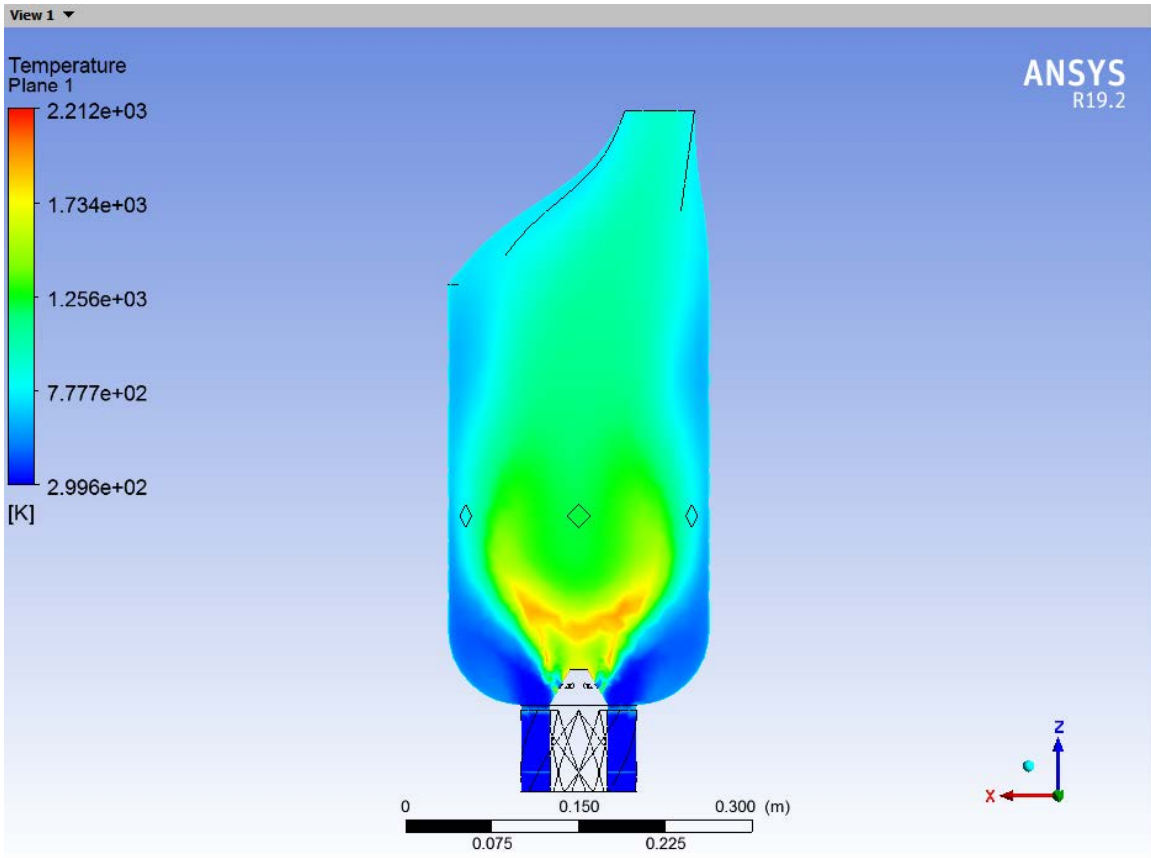
Temperature inside the combustion chamber (H$_2$-air reaction, inlet velocity 55 m/s)
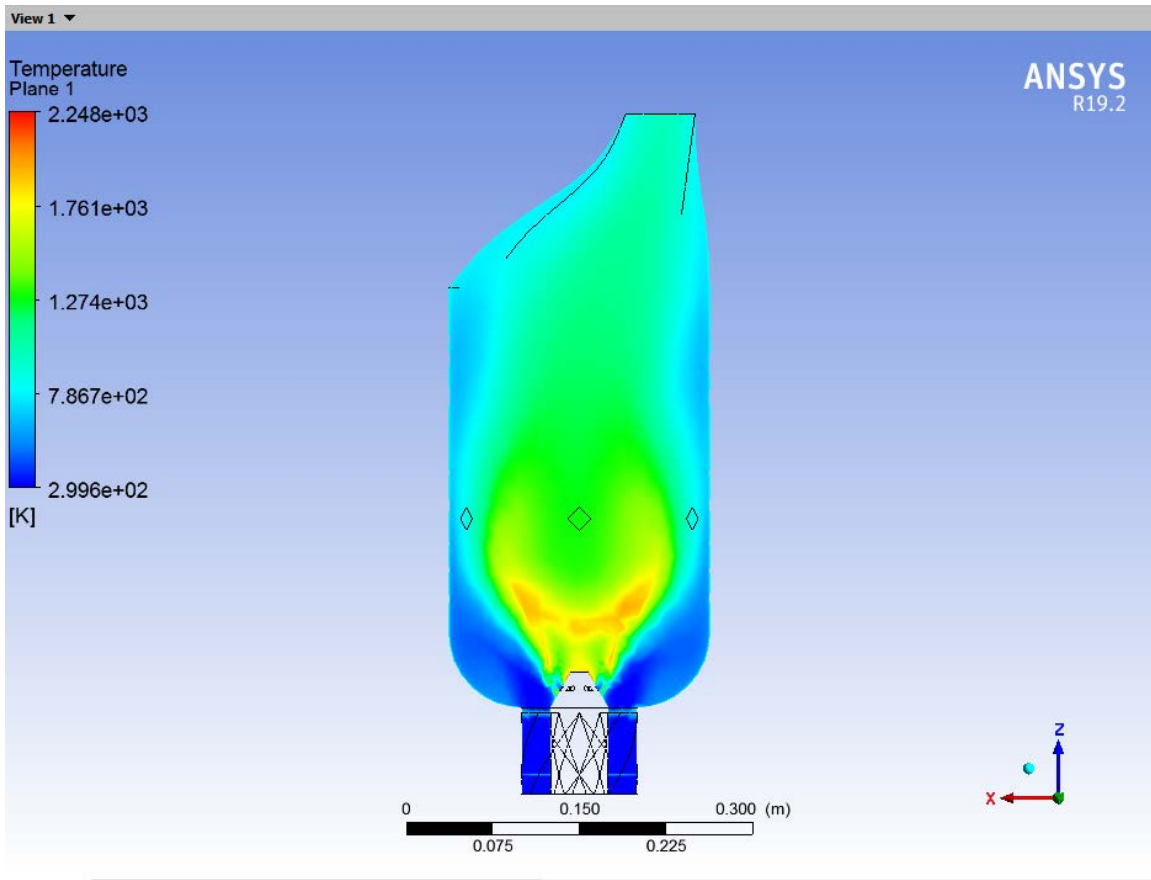
Temperature inside the combustion chamber (H_2-air reaction, inlet velocity 60 m/s)
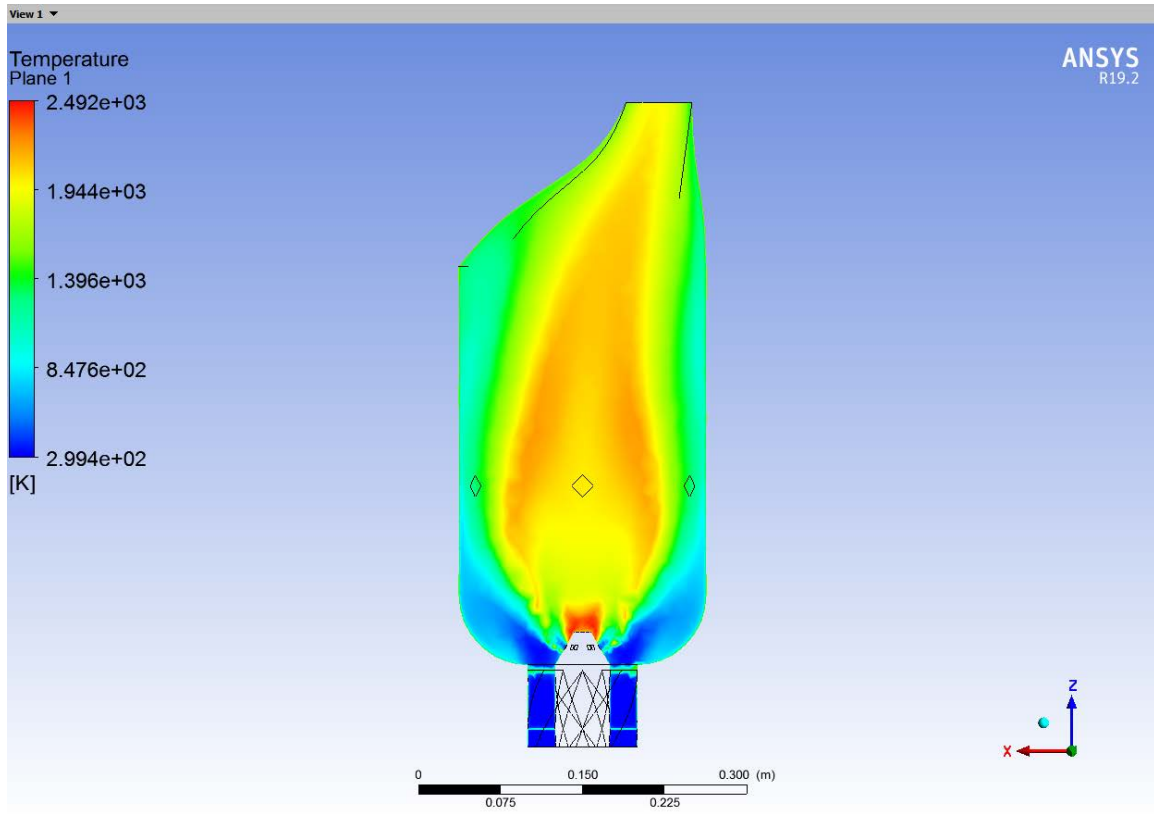
Temperature inside the combustion chamber (H$_2$-air reaction, inlet velocity 165 m/s)

# APPENDIX D. GASTURB INPUT AND OUTPUT DECKS

A.   NATURAL GAS INPUTS

Heat Exchanger	Exhaust Loss	Application	Steam Cooling	Water/Steam	Fuel:
Basic Data	Air System	Comp Efficiency	Comp Design	Turb Efficiency	Tip Clear.
Flight	Testbed	Power Generation			Natural Gas ⌄

Total Temperature T1	K	288.15
Total Pressure P1	kPa	101.325
Ambient Pressure Pamb	kPa	101.325
Relative Humidity [%]		0
Inlet Corr. Flow W2Rstd	kg/s	0.30745
Intake Pressure Ratio		0.99
Pressure Ratio		3.39
Burner Exit Temperature	K	1132
Burner Design Efficiency		0.9999
Burner Partload Constant		1.6
Fuel Heating Value	MJ/kg	49.7365
Overboard Bleed	kg/s	0
Mechanical Efficiency		0.9785
Burner Pressure Ratio		0.98
Turbine Exit Duct Press Ratio		0.98
Design Exhaust Pressure Ratio		1.03

Basic data inputs (natural gas, SI units)

Basic Data	Air System	Comp Efficiency	Comp Design	Turb Efficiency	Tip Clear.	Fuel:
Heat Exchanger	Exhaust Loss	Application	Steam Cooling	Water/Steam		Natural Gas ⌄

The Options:

○   1: w/o Heat Exchanger

◉   2: with Heat Exchanger (Method 1)

○   3: with Heat Exchanger (Method 2)

Heat Exchanger Effectiveness		0.8
Heat Exchanger Design P35/P3		0.99
Heat Exchanger Design P7/P6		0.9

Heat exchanger data inputs (natural gas, SI units)

Heat Exchanger		Exhaust Loss	Application		Steam Cooling		Water/Steam	Fuel:
Basic Data	Air System	Comp Efficiency		Comp Design	Turb Efficiency		Tip Clear.	Natural Gas ⌄
Rel. Handling Bleed					0			
Rel. Enthalpy of Handling Bleed					1			
Rel. Overboard Bleed W_Bld/W2					0.01			
Rel. Enthalpy of Overb. Bleed					1			
Recirculating Bleed W_reci/W2					Off Design Input Only			
Rel. Enthalpy of Recirc Bleed					1			
NGV Cooling Air W_Cl_NGV/W2					0.01			
Rotor Cooling Air W_Cl/W2					0			
Cooling Air Pumping Diameter			m		0			

Air system data inputs (natural gas, SI units)

Heat Exchanger		Exhaust Loss	Application		Steam Cooling		Water/Steam	Fuel:
Basic Data	Air System	Comp Efficiency		Comp Design	Turb Efficiency		Tip Clear.	Natural Gas ⌄

The Options:

◉ 1: isentropic

○ 2: polytropic

○ 3: calculate it

Isentr.Compr.Efficiency		0.787

Compressor efficiency data inputs (natural gas, SI units)

Heat Exchanger		Exhaust Loss		Application		Steam Cooling		Water/Steam
Basic Data	Air System	Comp Efficiency	Comp Design	Turb Efficiency	Tip Clear.

The Options:

○ 1: no

● 2: yes

Compressor Tip Speed	m/s	350
Compressor Inlet Radius Ratio		0.5
Compressor Inlet Mach Number		0.54
Engine Inl/Compr Tip Diam Ratio		1
min Compr Inlet Hub Diameter	m	0

Fuel:

Natural Gas ∨

Compressor design data inputs (natural gas, SI units)

Heat Exchanger		Exhaust Loss		Application		Steam Cooling		Water/Steam
Basic Data	Air System	Comp Efficiency	Comp Design	Turb Efficiency	Tip Clear.

The Options:

● 1: isentropic

○ 2: polytropic

○ 3: calculate it

Isentr.Turbine Efficiency		0.8555

Fuel:

Natural Gas ∨

Turbine efficiency data inputs (natural gas, SI units)

B. NATURAL GAS OUTPUTS

Summary | Compressor | Air System

```
              W         T         P       WRstd
Station     kg/s        K        kPa      kg/s        PWSD      =       28.4 kW
  amb               288.15    101.325
   1        0.304    288.15    101.325               PSFC      =      0.2877 kg/(kW*h)
   2        0.304    288.15    100.312    0.307       Heat Rate=   14308.2 kJ/(kW*h)
   3        0.304    439.90    340.057    0.112       Therm Eff=     0.2516
  31        0.301    439.90    340.057               WF        =     0.00227 kg/s
  35        0.298    819.38    336.656               P35/P3    =     0.99000
   4        0.301   1132.00    329.923    0.183       P7/P6     =     0.90000
  41        0.304   1129.01    329.923    0.185       s NOx     =     0.45507
  49        0.304    912.38    118.327               incidence=     0.00000 °
   5        0.304    912.38    118.327    0.464       XM8       =      0.2077
   6        0.304    912.38    115.961               A8        =      0.0049 m²
   7        0.304    549.89    104.365
   8        0.304    549.89    104.365    0.408       P8/Ps8    =     1.03000
Bleed       0.003    439.90    340.056               WBld/W2   =     0.01000
------------------------------------------------    P2/P1     =     0.99000
Efficiencies:   isentr   polytr     RNI     P/P       W_NGV/W2  =     0.01000
 Compressor     0.7870   0.8196   0.990   3.390       WCL/W2    =     0.00000
 Burner         0.9999                    0.980       Loading   =      100.00 %
 Turbine        0.8555   0.8387   0.656   2.788       e45 th    =     0.85543
 Heat Exch.     0.8000
 Generator      1.0000                                PW_gen    =       28.4 kW
------------------------------------------------
Spool mech Eff  0.9785   Nom Spd   127512 rpm         P6/P5     =      0.9800
------------------------------------------------


hum [%]      war0       FHV      Fuel
   0.0     0.00000     49.736    Natural Gas
```
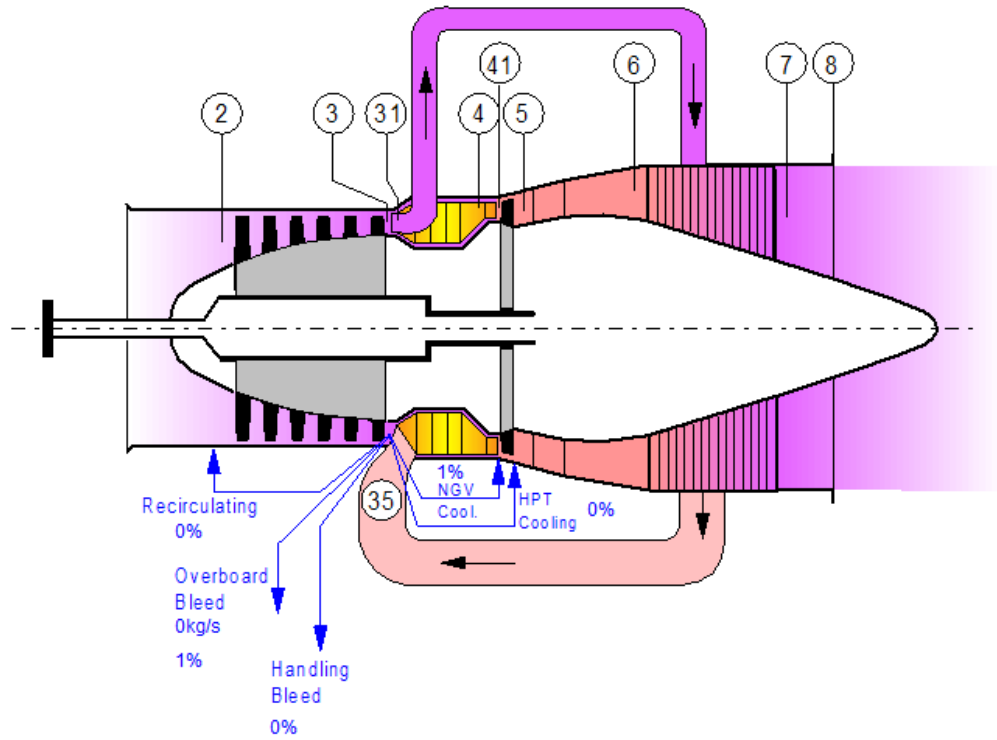
Summary of outputs (natural gas, SI units)

Summary | Compressor | Air System

```
 Input:
Compressor Tip Speed            m/s          350.00000
Compressor Inlet Radius Ratio                  0.50000
Compressor Inlet Mach Number                   0.54000
Engine Inl/Compr Tip Diam Ratio                1.00000
min Compr Inlet Hub Diameter    m              0.00000
 Output:
Compressor Tip circumf. Mach No                1.05803
Compressor Tip relative Mach No                1.18787
Design Spool Speed       [RPM]             127511.63
Compr Inlet Tip Diameter        m              0.05242
Compr Inlet Hub Diameter        m              0.02621
Calculated Compr Radius Ratio                  0.50000
Aerodynamic Interface Plane     m²             0.00216
Corr.Flow/Area Compr         kg/(s*m²)       189.92577
```

Compressor data outputs (natural gas, SI units)

Air system outputs (natural gas, SI units)
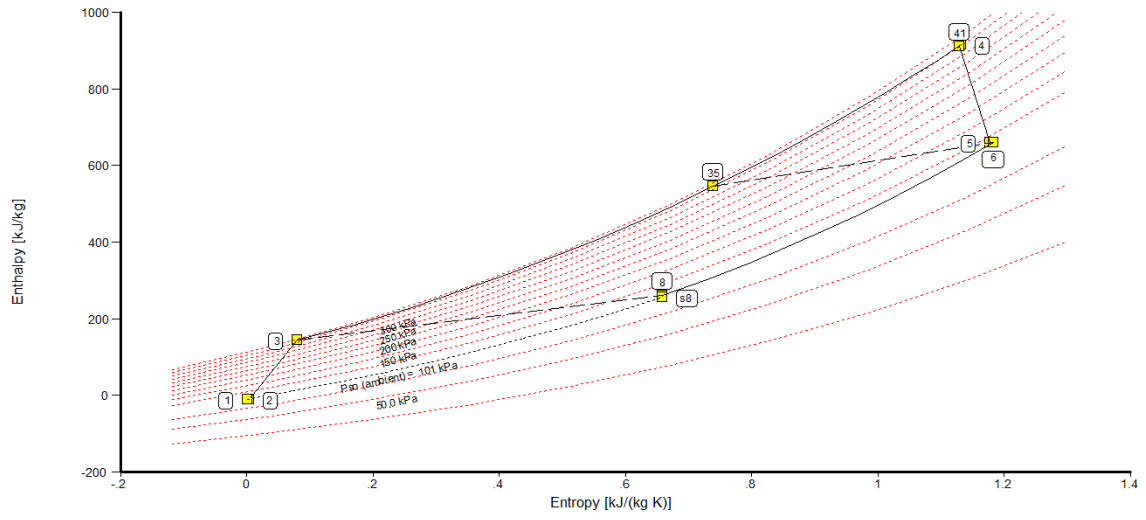
Enthalpy-entropy diagram (natural gas, SI units)
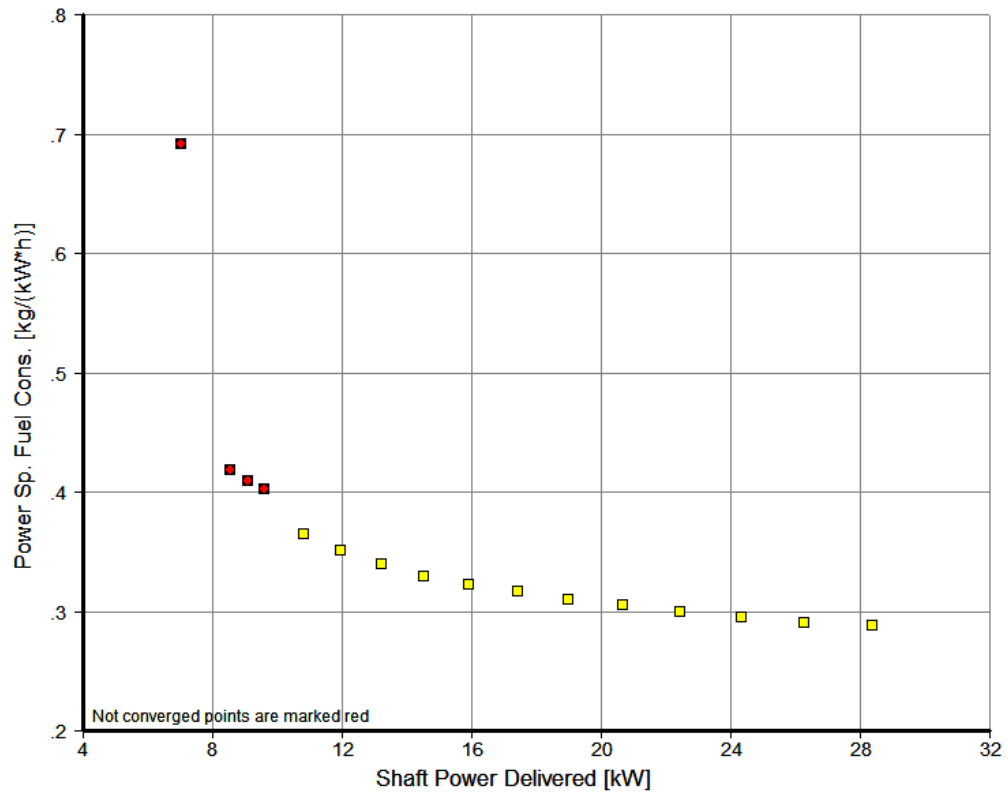
Shaft power delivered-power specific fuel consumption diagram

(natural gas, SI units)

C. HYDROGEN INPUTS

Basic data inputs (H$_2$, SI units)

Heat exchanger data inputs (H$_2$, SI units)

70

Heat Exchanger	Exhaust Loss	Application	Steam Cooling	Water/Steam
Basic Data	Air System	Comp Efficiency	Comp Design	Turb Efficiency	Tip Clear.

Rel. Handling Bleed		0
Rel. Enthalpy of Handling Bleed		1
Rel. Overboard Bleed W_Bld/W2		0.01
Rel. Enthalpy of Overb. Bleed		1
Recirculating Bleed W_reci/W2		Off Design Input Only
Rel. Enthalpy of Recirc Bleed		1
NGV Cooling Air W_Cl_NGV/W2		0.01
Rotor Cooling Air W_Cl/W2		0
Cooling Air Pumping Diameter	m	0

Fuel: Hydrogen

Air system data inputs (H$_2$, SI units)

Heat Exchanger	Exhaust Loss	Application	Steam Cooling	Water/Steam
Basic Data	Air System	Comp Efficiency	Comp Design	Turb Efficiency	Tip Clear.

The Options:
- ⦿ 1: isentropic
- ○ 2: polytropic
- ○ 3: calculate it

Isentr.Compr.Efficiency		0.787

Fuel: Hydrogen

Compressor efficiency data inputs (H$_2$, SI units)

Heat Exchanger	Exhaust Loss	Application	Steam Cooling	Water/Steam	Fuel:
Basic Data	Air System	Comp Efficiency	Comp Design	Turb Efficiency	Tip Clear.	Hydrogen

The Options:

○ 1: no

● 2: yes

Compressor Tip Speed	m/s	350
Compressor Inlet Radius Ratio		0.5
Compressor Inlet Mach Number		0.54
Engine Inl/Compr Tip Diam Ratio		1
min Compr Inlet Hub Diameter	m	0

Compressor design data inputs (H_2, SI units)

Heat Exchanger	Exhaust Loss	Application	Steam Cooling	Water/Steam	Fuel:
Basic Data	Air System	Comp Efficiency	Comp Design	Turb Efficiency	Tip Clear.	Hydrogen

The Options:

● 1: isentropic

○ 2: polytropic

○ 3: calculate it

Isentr.Turbine Efficiency		0.8555

Turbine efficiency data inputs (H_2, SI units)

D. HYDROGEN OUTPUTS

```
Summary  Compressor  Air System

           W         T         P       WRstd
Station  kg/s       K        kPa       kg/s        PWSD     =       29.0 kW
 amb               288.15   101.325
  1      0.304     288.15   101.325               PSFC     =     0.1185 kg/(kW*h)
  2      0.304     288.15   100.312    0.307       Heat Rate=  14029.1 kJ/(kW*h)
  3      0.304     439.94   340.057    0.112       Therm Eff=    0.2566
 31      0.301     439.94   340.057               WF       = 9.5548E-4 kg/s
 35      0.298     818.80   336.656               P35/P3   =    0.99000
  4      0.299    1132.00   329.923    0.184       P7/P6    =    0.90000
 41      0.302    1129.02   329.923    0.185       s NOx    =    0.45370
 49      0.302     911.64   118.327               incidence=    0.00000 °
  5      0.302     911.64   118.327    0.464       XM8      =    0.2078
  6      0.302     911.64   115.961               A8       =    0.0049 m²
  7      0.302     551.80   104.365
  8      0.302     551.80   104.365    0.410       P8/Ps8   =    1.03000
Bleed    0.003     439.94   340.056               WBld/W2  =    0.01000
-------------------------------------------       P2/P1    =    0.99000
Efficiencies:  isentr  polytr    RNI    P/P       W_NGV/W2 =    0.01000
 Compressor    0.7870  0.8195  0.990  3.390       WCL/W2   =    0.00000
 Burner        0.9999                 0.980       Loading  =   100.00 %
 Turbine       0.8555  0.8386  0.655  2.788       e45 th   =    0.85541
 Heat Exch.    0.8000
 Generator     1.0000                             PW_gen   =      29.0 kW
-------------------------------------------
Spool mech Eff 0.9785  Nom Spd   127511 rpm       P6/P5    =    0.9800
-------------------------------------------

hum [%]     war0        FHV      Fuel
  0.0     0.00000     118.429    Hydrogen
```

Summary of outputs (H$_2$, SI units)

```
Summary  Compressor  Air System

 Input:
Compressor Tip Speed            m/s          350.00000
Compressor Inlet Radius Ratio                  0.50000
Compressor Inlet Mach Number                   0.54000
Engine Inl/Compr Tip Diam Ratio                1.00000
min Compr Inlet Hub Diameter    m              0.00000
 Output:
Compressor Tip circumf. Mach No                1.05803
Compressor Tip relative Mach No                1.18787
Design Spool Speed       [RPM]             127511.03
Compr Inlet Tip Diameter     m                 0.05242
Compr Inlet Hub Diameter     m                 0.02621
Calculated Compr Radius Ratio                  0.50000
Aerodynamic Interface Plane   m²               0.00216
Corr.Flow/Area Compr      kg/(s*m²)          189.92399
```

Compressor data outputs (H$_2$, SI units)

73
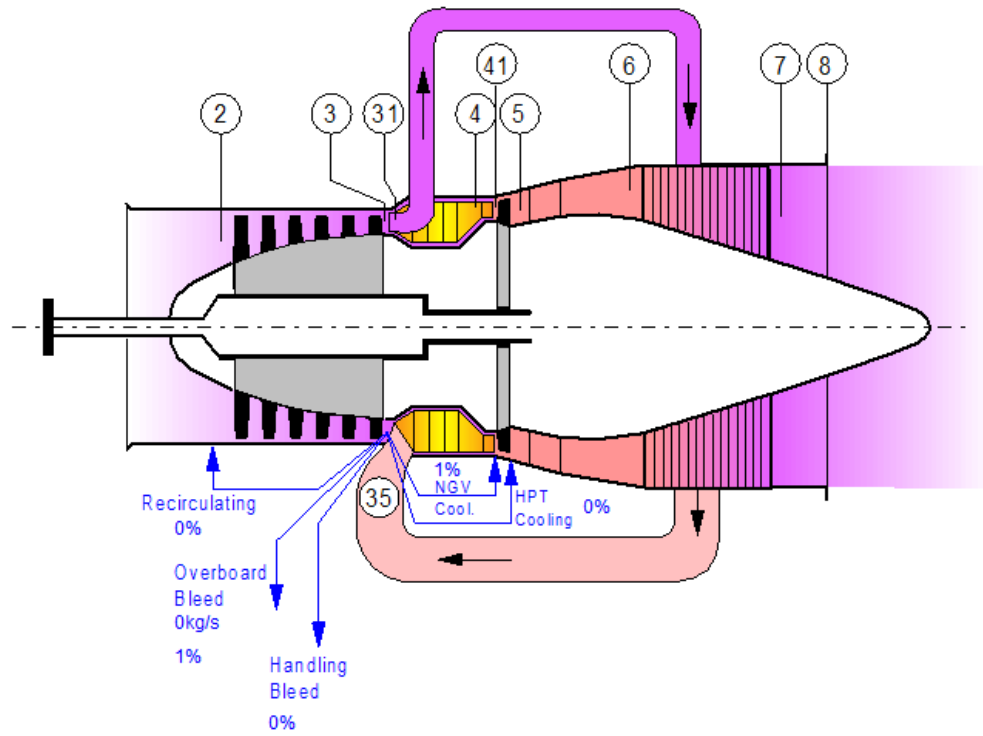
Air system outputs (H$_2$, SI units)
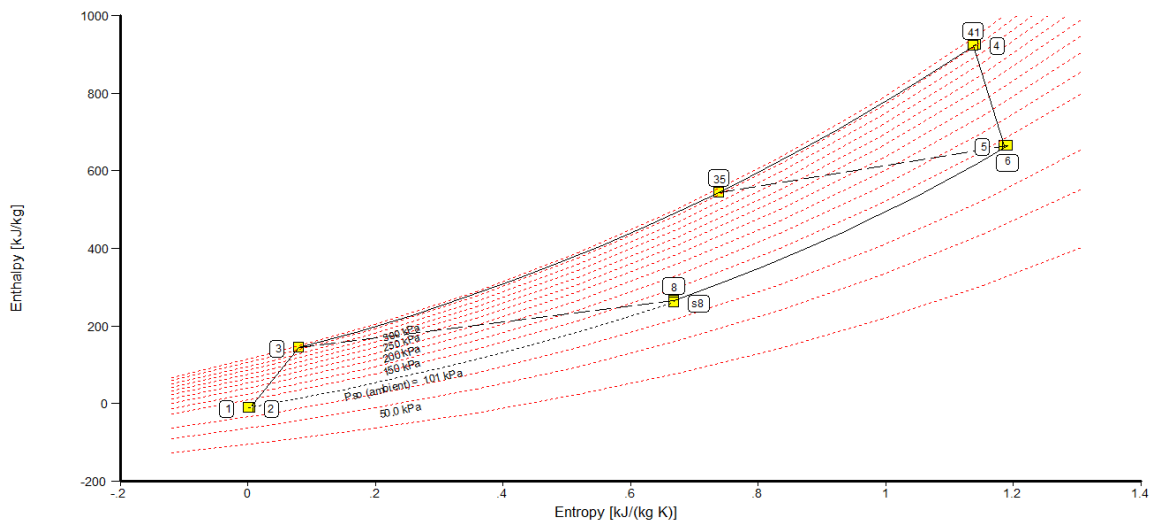
Enthalpy-entropy diagram (H$_2$, SI units)
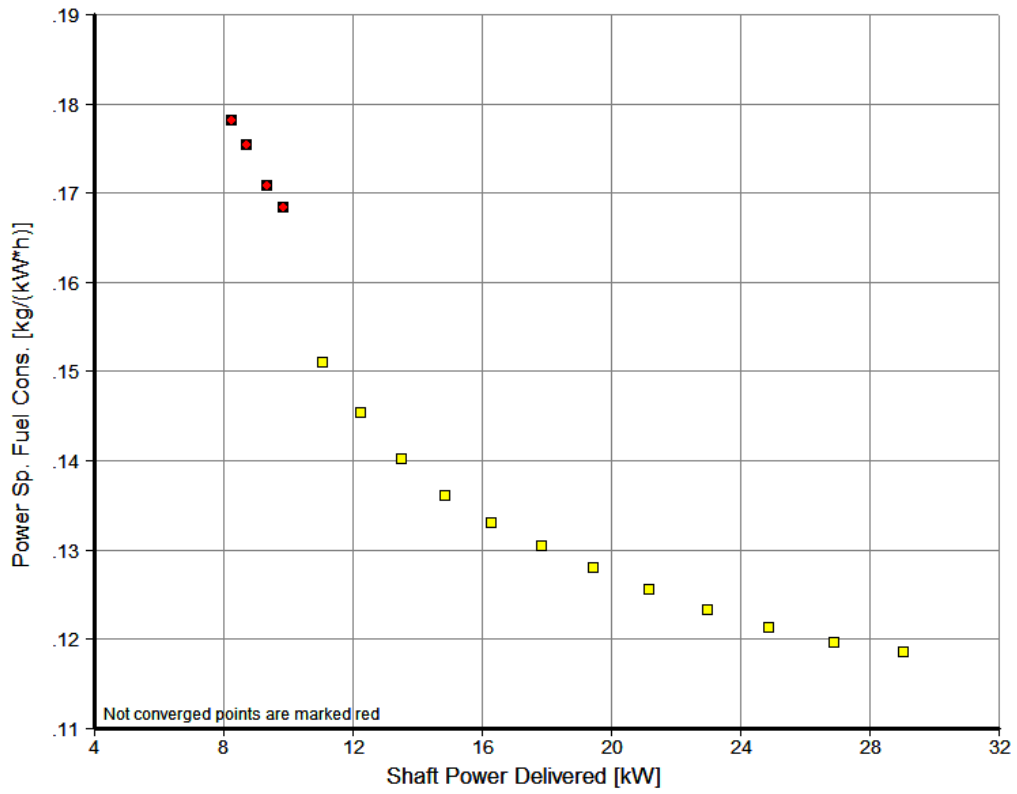
Shaft power delivered-power specific fuel consumption diagram (H$_2$, SI units)

75

THIS PAGE INTENTIONALLY LEFT BLANK

APPENDIX E. PROCEDURE FOR OPERATING WITH HYDROGEN

1. Verify that there are no leaks and that no power is supplied to the solenoid valves.

2. Move the battery isolation switch to the ON position, accessible via the panel labeled "BATERY CIRCUIT BREAKER ACCESS SWITCH" [14].

3. Press the "BATT START" button (accessible via the control panel, labeled with the Capstone logo) to wake the C30 from sleep mode [14].

4. Verify that the C30 is configured for Stand Alone Operation. If not already in Stand Alone Operation Mode, configure the C30 as described in chapter 3 of reference [14] and in reference [16].

5. Start the CRMS software, previously installed on a laptop with a RS-232 serial port [17].

6. Connect the computer to the C30 and establish communications. Open the Communications Bay to access the User Connection Board and the User Port (J6) in accordance with section 2.1, User Interface [14]. Connect the computer' RS-232 serial port to the C30 RS-232 serial port using a null modem cable. Attempts to extend the cable by connecting it in series with another modem cable are not recommended.

7. Select the "Display" tab from the options bar in the "Unit_1" window. Select "Strip Chart."

8. Once the chart labelled "Microturbine Chart, Unit_1" appears, select the desired parameters from the drop down menus. No more than four parameters are recommended to avoid visual clutter unless specifically required for real-time observation. All parameters will have data collected and may be charted/graphed later. The recommended parameters are "Turbine Exit Temperature," "Battery SOC," "Compressor Inlet Temperature", and "Engine Speed" for a no-load run. Adjust the number of points to cover the expected runtime of the turbine. Beneath each parameter, select the upper and lower bounds. The y-axis ranges from 0 to 1, with each parameter

being charted as a decimal percentage of its upper bound [17]. Recommend zero to above maximum value achieved. Avoid setting expected values such that multiple parameters chart at similar values (i.e., 0.8 for both TET and Bat SOC).

9. Select "Control Mode" from the mode drop-down menu. If prompted for a password, enter the default user port user password <USR123P> or the selected user port user password [17].

10. Select the save/"File Manager" button in the top ribbon. The toggle button "Recording" should be set to manual within the "Data Recording" pane. Click the radio button "Start Recording" within the same pane; when it appears green and says "ON," close the window. The file location may also be changed to user preference.

11. Manually open the H_2 tank valve and the manual shutoff valve.

12. Adjust the regulator to the desired fuel supply pressure.

13. Evacuate the area. (One of the test cells at the TPL was used to provide a safe barrier between the C30 and the user in the event of uncontrolled combustion.)

14. Open solenoid valve 1 remotely.

15. Open solenoid valve 2 remotely and vent for 2-4 seconds to flush the supply system with H_2 and reduce the chance of flashback.

16. Close solenoid valve 2 remotely.

17. Click "START" under "Turbine Start" and allow the C30 to start up and run [17].

18. Observe data collection/conduct experiment.

19. Click "STOP" under "Turbine Start" and allow the C30 to run its shutdown procedure. In the event of an automatic shutdown and an error message, allow the C30 to safely stop on its own [17].

20. Verify that the C30 has stopped.

21. Close solenoid valve 1 remotely.

22. Vent the remaining H_2 in the supply line by actuating solenoid valve 2 remotely.

23. Close the manual shutoff valve and the H_2 tank valve.

24. Turn off the control panel by moving the battery isolation switch into the OFF position, accessible via the panel labeled "BATERY CIRCUIT BREAKER ACCESS SWITCH" [14].

25. Save the collected data and disconnect the computer from the C30.

THIS PAGE INTENTIONALLY LEFT BLANK

APPENDIX F. FUEL HEATING VALUES

Using the ideal gas law, a fuel's molar mass, and a fuel's heating value on a per unit mass basis, the fuel's heating value per unit volume was calculated. H_2 requires a volume flow rate over three times that of natural gas to provide the same thermal energy at a constant pressure and temperature.

$$pV = nRT$$

$$\frac{p}{RT} = \frac{n \cdot MM}{V}$$

$$\rho = \frac{p}{RT}$$

$$HHV_{vol} = \frac{HHV_{mass}}{\rho}$$

$$HHV_{vol} = HHV_{mass} * \frac{RT}{p}$$

Molar Mass [g/mol] [12]	HHV [kJ/kg] [12]	LHV [kJ/kg] [12]	Density at 20ºC, 379 kPa	HHV [kJ/m³]	LHV[kJ/m³]
2.016 (H_2)	141781	119953	0.3138	44492	37642
16.043 (CH_4)	55496	50010	2.497	138578	124879
44.094 (C_3H_8)	50343	46352	6.862	345471	218084

THIS PAGE INTENTIONALLY LEFT BLANK

LIST OF REFERENCES

[1]   J.I. Levene, M.K. Mann, R. Margolis, and A. Milbrandt, "An analysis of hydrogen production from renewable electricity sources," National Renewable Energy Laboratory, Golden, CO, USA 2005. [Online] Available: https://www.nrel.gov/docs/fy05osti/37612.pdf

[2]   E. Tzimas, C. Filiou, S.D. Peteves, and J.B. Veyret, "Hydrogen storage: State-of-the-art and future perspective," European Commission Joint Research Center Institute for Energy, Petten, the Netherlands, 2003. [Online] Available: https://pdfs.semanticscholar.org/1fc0/398a56d147790df6b8af9aab677e1c04eeb6.pdf

[3]   Energy Policy Act of 2005, Pub. L. No. 109–58, [Online]. Available: https://www.gps.gov/fdsys/pkg/PLAW/109publ58/pdf/PLAW-109pub158.pdf

[4]   S. Birkemeier, "Industrial automation of solar-powered hydrogen generation plant," M.S. thesis, Mech. Egr. Dept., Naval Postgraduate School, Monterey, CA, USA 2018. [Online] Available: https://calhoun.nps.edu/handle/10945/59700

[5]   E.A. Fosson, "Design and analysis of a hydrogen compression and storage station," M.S. thesis, Mech. Egr. Dept., Naval Postgraduate School, Monterey, CA, USA 2017. [Online] Available: https://calhoun.nps.edu/handle/10945/56919

[6]   A. Aviles, "Renewable production of water, hydrogen, and power from ambient moisture," M.S. thesis, Mech. Egr. Dept., Naval Postgraduate School, Monterey, CA, USA 2016. [Online] Available: https://calhoun.nps.edu/handle/10945/51584

[7]   J. Penley, "Gas turbine operation on compressed hydrogen," M.S. thesis, Mech. Egr. Dept., Naval Postgraduate School, Monterey, CA, USA 2018. [Online] Available: https://calhoun.nps.edu/handle/10945/51584

[8]   M. Melania and J. Eichman, "Hydrogen energy storage: grid and transportation services," National Renewable Energy Laboratory, Golden, CO, USA 2015. [Online] Available: https://www.nrel.gov/docs/fy15osti/62518.pdf

[9]   World Nuclear Association, "Nuclear process heat for industry," World Nuclear Association, London, UK 2018. [Online] Available: https://www.world-nuclear.org/information-library/non-power-nuclear-applications/industry/nuclear-process-heat-for-industry.aspx

[10]   *ANSYS CFX Tutorials*, 16th ed. ANSYS, Canonsburg, PA, USA, 2013.

[11]   *ANSYS CFX-Solver Theory Guide*, 15th ed. ANSYS, Canonsburg, PA, USA, 2013.

[12]   S. Turns, *An Introduction to Combustion: Concepts and Applications*. New York: McGraw Hill Education, 2012.

[13]   A. Gimelli and R. Sannino, "Thermodynamic model validation of Capstone C30 Micro Gas Turbine," *Energy Procedia*, vol. 126, pp. 955–962, Lecce, Italy, 2017.

[14]   "400001-001 Rev. C: Capstone MicroTurbine User's Manual," Capstone Turbine Corporation, Chatsworth, CA, USA, 2005.

[15]   "410037-001 Rev B: Gaseous System Technical Information" Capstone Turbine Corporation, Chatsworth, CA, USA, 2006.

[16]   "410028 Rev D: Stand Alone Operation – Capstone Model C30 and C60/C65," Capstone Turbine Corporation, Chatsworth, CA, USA, 2006.

[17]   "410013 Rev U: Capstone Remote Monitoring System (User Edition)," Capstone Turbine Corporation, Chatsworth, CA, USA, 2017.

INITIAL DISTRIBUTION LIST

1.   Defense Technical Information Center
        Ft. Belvoir, Virginia

2.   Dudley Knox Library
        Naval Postgraduate School
        Monterey, California